Applied Thermal Engineering 145 (2018) 80–97

Contents lists available at ScienceDirect

Applied Thermal Engineering

journal homepage: www.elsevier.com/locate/apthermeng

Research Paper

Fluid-structure interaction in natural convection heat transfer in an oblique cavity with a flexible oscillating fin and partial heating

A.I. Alsabery[a,b,*], M.A. Sheremet[c], M. Ghalambaz[d], A.J. Chamkha[e,f], I. Hashim[b]

[a] Department of Refrigeration & Air-conditioning Technical Engineering, College of Technical Engineering, The Islamic University, Najaf, Iraq
[b] School of Mathematical Sciences, Faculty of Science & Technology, Universiti Kebangsaan Malaysia, 43600 UKM Bangi, Selangor, Malaysia
[c] Department of Theoretical Mechanics, Tomsk State University, 634050 Tomsk, Russia
[d] Department of Mechanical Engineering, Dezful Branch, Islamic Azad University, Dezful, Iran
[e] Department of Mechanical Engineering, Prince Sultan Endowment for Energy and the Environment, Prince Mohammad Bin Fahd University, Al-Khobar 31952, Saudi Arabia
[f] RAK Research and Innovation Center, American University of Ras Al Khaimah, P.O. Box 10021, Ras Al Khaimah, United Arab Emirates

HIGHLIGHTS

- FEM and Arbitrary Lagrangian-Eulerian (ALE) procedure are used in the numerical analysis.
- Two different heating sources are places in various locations within the oblique cavity.
- The developed computational code is validated comprehensively using the previous numerical data.
- The obtained results revealed an essential effect of the fin on the flow and heat transfer.

ARTICLE INFO

Keywords:
Natural convection
Flexible oscillating heat-conducting fin
Oblique cavity
Local isothermal heater

ABSTRACT

Unsteady natural convection in a differentially heated oblique cavity with a flexible oscillating heat-conducting fin mounted on the bottom adiabatic wall is studied numerically by using the finite element method. The right inclined wall is kept at a constant low temperature, while the left one is adiabatic with a local isothermal heater, the fin is heated isothermally from the basis. The heat-conducting elastic fin is located in the central part of the bottom adiabatic wall. The Galerkin weighted residual finite element method with the aid of the Arbitrary Lagrangian-Eulerian (ALE) procedure is used in the numerical analysis. The developed computational code was validated comprehensively using a grid independency test, and numerical data of other authors. The governing parameters of this study are the dimensionless time ($10^{-8} \leqslant t \leq 3.5$), thermal conductivity ratio between the heat-conducting fin and working medium ($1 \leqslant K_r \leq 1000$), non-dimensional Young's modulus ($10^9 \leqslant E \leq 10^{12}$), oscillating amplitude ($0.01 \leqslant A \leqslant 0.1$), left wall heater length ($0.1 \leqslant H \leq 0.9$), and the inclination angle of tilted walls ($-45 \leqslant \phi \leqslant 45$). The obtained results revealed an essential effect of the flexible oscillating heat-conducting fin on the fluid flow and heat transfer inside the oblique cavity.

1. Introduction

The important phenomenon of natural convective heat transfer in industrial and engineering systems can be observed from the wide applications, such as cooling of electronic components, heat exchangers, double pane windows and cooling systems in nuclear reactors. Natural convective flow and heat transfer occur within cavities due to the temperature difference and buoyancy forces. A comprehensive review on natural convection in different cavities with various shapes and configurations was reported by Ostrach [1]. The Fluid Structure Interaction (FSI) is the study of the interaction of a moveable or deformable surface with a fluid. In FSI problems, the fluid domain is subject to a continuous change (deformation) due to the transformation shape of the moveable or deformable surface. One way to track the deformation of the fluid space is using the moving grid. In the moving grid method, the grid points are relocated by Lagrangian transport to match the moving or deformable surfaces. Recently, excellent books have been published on the subject of FSI [2–6].

* Corresponding author at:School of Mathematical Sciences, Faculty of Science & Technology, Universiti Kebangsaan Malaysia, 43600 UKM Bangi, Selangor, Malaysia.
E-mail address: ammar_e_2011@yahoo.com (A.I. Alsabery).

https://doi.org/10.1016/j.applthermaleng.2018.09.039
Received 27 June 2018; Received in revised form 4 September 2018; Accepted 8 September 2018
Available online 10 September 2018
1359-4311/

Nomenclature

A	dimensionless amplitude of the fin
b	thickness of the fin
E	dimensionless Young's modulus
F_v	dimensionless body force vector
g	gravitational acceleration
H	dimensionless length of the heater
k	thermal conductivity
K_r	thermal conductivity ratio of the solid to the fluid
L	width and height of cavity
$\overline{Nu}$	average Nusselt number
Pr	Prandtl number
Ra	Rayleigh number
S	stress tensor
t	dimensionless time
T	temperature
u^*, v^*	velocity components in the x-direction and y-direction
u, v	dimensionless velocity components in the X-direction and Y-direction
x, y & X, Y	space coordinates & dimensionless space coordinates

Greek symbols

α	thermal diffusivity
β	thermal expansion coefficient
λ	Frequency of the oscillation
ε	strain
θ	dimensionless temperature
μ	dynamic viscosity
ν	kinematic viscosity
ρ	density
σ	stress tensor
τ	dimensionless period of oscillation
ϕ	inclination angle of the sloping wall
Ψ	dimensionless stream function

subscript

c	cold
f	fluid
h	hot
r	the property ratio of the solid to the fluid
s	solid

There are many engineering cases in which the deformation of the moveable surface due to the interaction with the fluid is negligible. In such problems, the couple between the fluid and the structure is one way coupling. However, there are also many engineering problems in which the interaction of the fluid with the structure is important. In such problems, the fluid would affect the shape of the structure and at the same time, the shape of the structure would affect the fluid flow and its characteristics. These problems are two way coupling. Considering the one-way coupling of the fluid and structure interaction. Öztop and Dagtekin [7] considered the problem of steady mixed convection in a double lid-driven vertically heated square cavity. They concluded that the heat transfer was enhanced by moving the vertical walls in the opposite direction, while it was reduced by the movement of the walls in the same direction. The problem of mixed convection flow and heat transfer in a lid-driven top wall square cavity filled with copper-water nanofluid was investigated by Talebi et al. [8]. They used the finite volume method for solving the dimensionless governing equations and the found that the buoyancy effect and the flow intensity were increased with the augmentation of Rayleigh number. Abu-Nada and Chamkha [9] made a numerical study on the mixed convection flow in an inclined square cavity with a hot top lid-driven wall filled water-Al_2O_3 nanofluid. Their study concluded that the effect of Richardson number was strongly enhanced the heat transfer and the fluid flow. Rashad et al. [10] have studied the mixed convection of a micropolar fluid over a moving surface. They solved the governing ODE numerically using the Keller box method and they explained that the increment of the chemical reaction parameter led to the reduction of Nusselt number. Ramesh et al. [11] have extended the study of [10] to the case of mixed convection over an inclined moving surface. Where they observed that the temperature of the fixed flat plate was much higher than that of the moving flat plate. In a very recent work, Raju et al. [12] have taken into account unsteady effects for the problem of mixed convection over a moving surface. They concluded that the distribution of the velocity was an increasing function of Soret number. Chamkha et al. [13] as well as Alsabery et al. [14] have studied the mixed convection of a nanofluid in a lid-driven cavity. The top and bottom walls of the cavity was moving with the constant velocity of V. Kareem and Gao [15] have considered the 3D geometry of cavity with a sliding led. There are also many other researches which have studied the problems involving the moving wall or sliding wall. In all of these studies [7–15] the wall was symmetric and smooth, and hence, its motion was simply modeled by a non-zero velocity boundary condition whit out any need for the grid motion. Hence, all of these studies are one-way coupling in which the interaction between the wall and the fluid would not affect the shape of the wall.

In contrast with the mentioned studies of [7–15], there are some very recent studies in which the couple between the fluid and the structure is a two-way couple. Hence, the interaction between the fluid and the boundary not only affects the fluid but also the structure. Using the finite volume method, Shi and Khodadadi [16] and Shi and Khodadadi [17] numerically studied the problem of fluid flow and heat transfer in a lid-driven square cavity with an oscillating thin fin extruded from the right vertical wall of the cavity. Ku [18] in a patent has reported a new type of flexible heat sink which allow its parts to slightly deform due to the exerted force. The heat sink is composed of a flexible base which absorbs the heat from a hot component. The side opposite of the heat sink is covered with a plurality of groups of fins which are positioned in an array and spaced apart across the base and enabling the heat sink to flex lengthwise and width wise. Soti et al. [19] numerically investigated the flow-induced deformation of thin flexible structures coupled with convective heat transfer where they demonstrated a large-scale flow-induced deformation as an effective passive

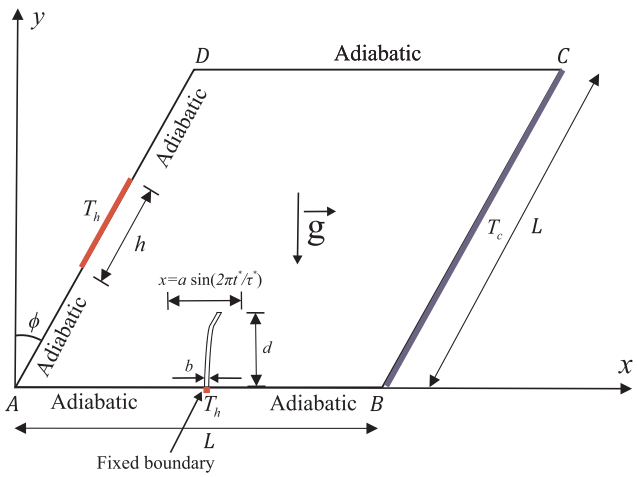

Fig. 1. Physical model of convection in an oblique cavity with a flexible oscillating fin and coordinate system.

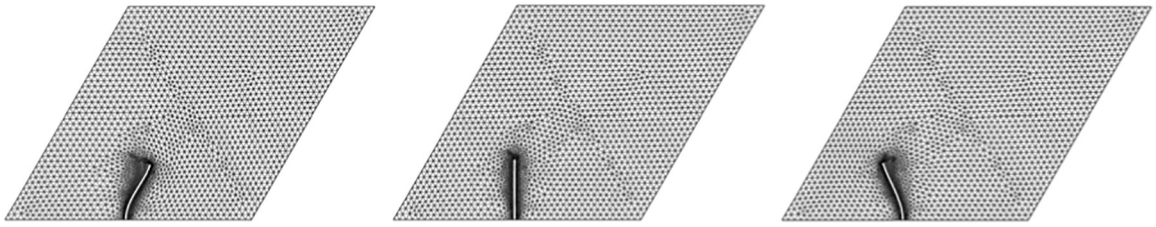

Fig. 2. Grid-points distribution for a grid size G6 = 6936.

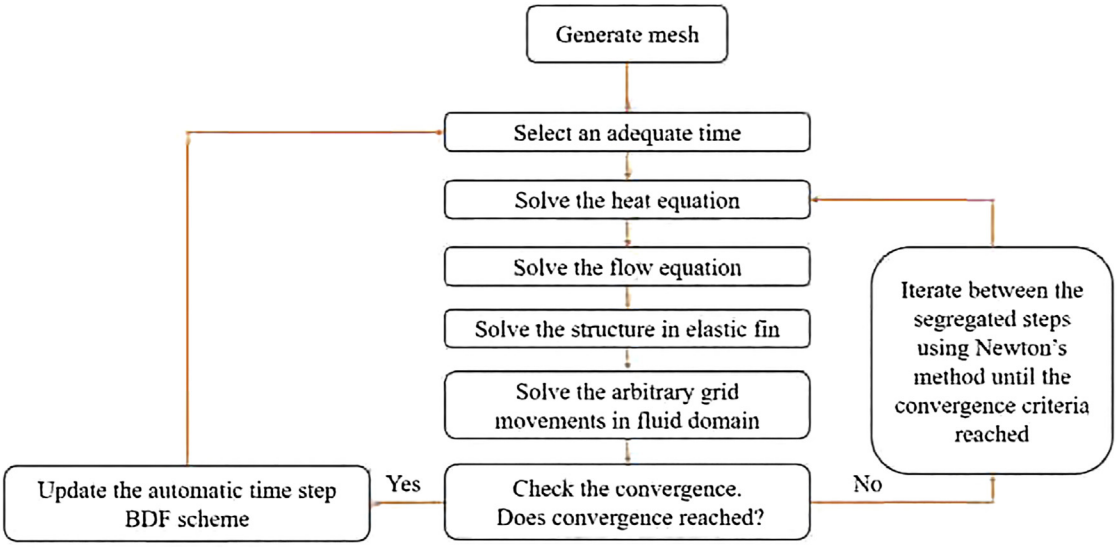

Fig. 3. The flowchart of the utilized numerical code.

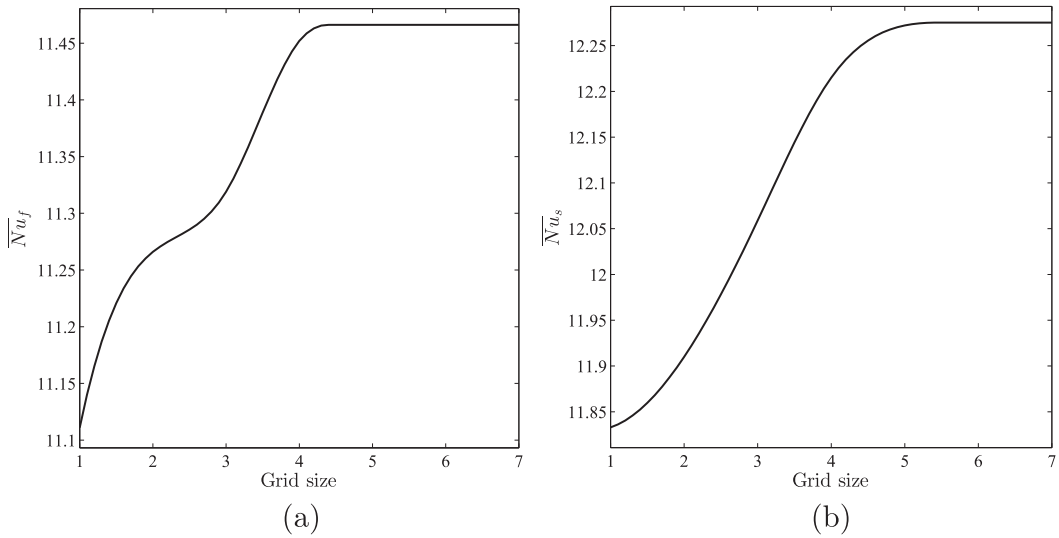

Fig. 4. Grid testing of the average Nusselt number on (a) the inclined left wall and (b) the solid fin with different grid sizes for $t = 3.5$, $Ra = 10^6$, $K_r = 10$, $E = 10^{11}$, $A = 0.1$, $H = 0.5$ and $\phi = 30$.

heat transfer enhancement technique. Selimefendigil and Öztop [20] studied numerically the effect of magnetic field on mixed convection heat transfer in a lid-driven square cavity filled with nanofluid in the presence of flexible left wall and volumetric heat generation. They reported that for high Richardson numbers, the average Nusselt number tended to increase as with Young's modulus of the elastic wall raised. Selimefendigil et al. [21] explained the Fluid-structure-magnetic field interaction in a lid-driven square cavity filled with CuO-water nanofluid and having flexible side wall. They concluded that the heat transfer rate was enhanced with the reduction of Young's modulus. Ghalambaz et al. [22] have studied the effect of the presence of an oscillating flexible fin in a cavity. The side walls of the cavity was isothermal with a temperature difference and the top and bottom walls was well insulated. The fin was highly thermal conductive and was mounted at the hot wall. The results show that the flexibility, the oscillation frequency and the amplitude of the fin can affect the heat transfer in the cavity. However, the presence of a horizontal fin can negatively block the natural convection fluid flow circulation, and hence, the presence of the

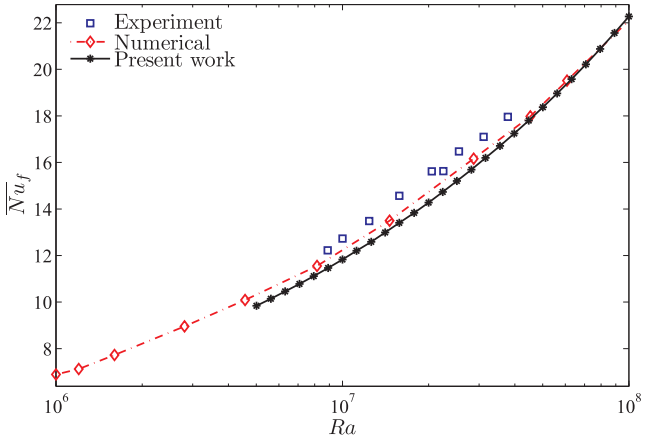

Fig. 5. Comparison between the average Nusselt number of the current numerical work and the experimental data demonstrated by Nishimura et al. [40] and the numerical work based on Churchill's relation by Churchill [41] with Rayleigh number for a rectangular cavity when $AR = 4$ and Pr = 6.

oscillating fin did not induce a significant enhancement of heat transfer in the cavity. Very recently, Selimefendigil and Öztop [23] and Selimefendigil et al. [24] have studied the convective heat transfer by considering a flexible boundary surface over a backward-facing step with an elastic bottom as well as a cavity with a flexible side wall. In these two studies the boundary surfaces are flexible, and hence, the interaction between the fluid and the surface would affect both of the surface and fluid flow. Raisi and Arvin [25] have studied the effect of the presence of a flexible horizontal baffle inside a cavity. In this study the flexible component has been embedded in the domain. The baffle in the cavity was subject to small deformations due to the interaction with the fluid. As a result, the deformation of the baffle affect the fluid flow in the cavity. The results show that the flexibility of the baffle and its size affects the convection heat transfer in the cavity. Selimefendigil et al. [26] used the finite element method to investigate the problem of MHD mixed convection heat transfer in a lid-driven square cavity filled with nanofluid in the presence of flexible fin connected to the top wall. They observed an enhancement on the heat transfer as the solid volume fraction increased in the exist of the flexible fin. Ismael and Jasim [27] have extended the problem to the study of mixed convection in an open cavity in the presence of a flexible fin subject to the incoming fluid flow. The results show that a flexible fin can enhance the heat transfer rate compared to a rigid one. They also reported that the shape of the fin and the heat transfer rate for strong mixed convection flows show a periodic behavior.

In reality, convection heat transfer in cavities is a prototype for a great number of industrial applications, and especially, non-rectangular cavities (trapezoidal, oblique) which has the attention of many research papers due to the wide applications in various fields. The moderately concentrating solar energy collector is an important example involving an oblique (parallelogrammic) geometry. Natural convection heat

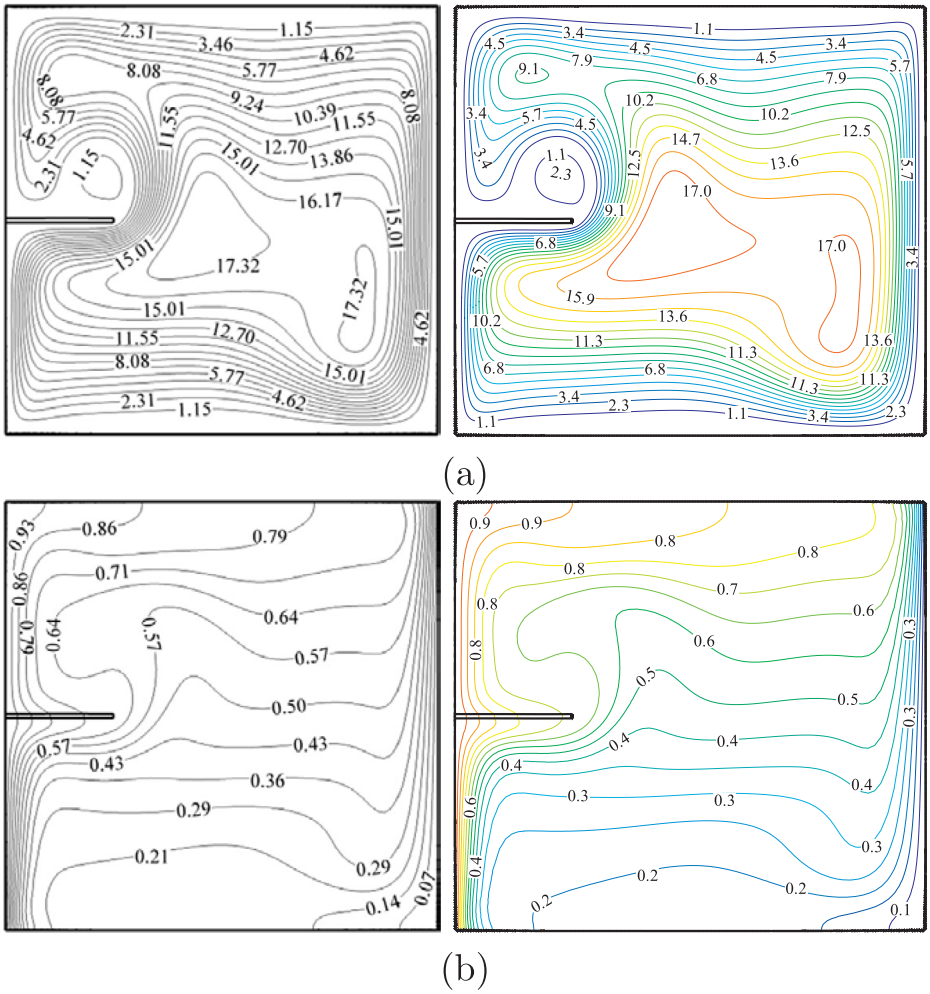

Fig. 6. Streamlines (a), Ghalambaz et al. [22] (left), present study (right), isotherms (b), Ghalambaz et al. [22] (left), present study (right) for $Ra = 10^6$, $E = 10^{11}$, $A = 0.1$, $H = 1$, $\phi = 0$ and Pr = 0.7.

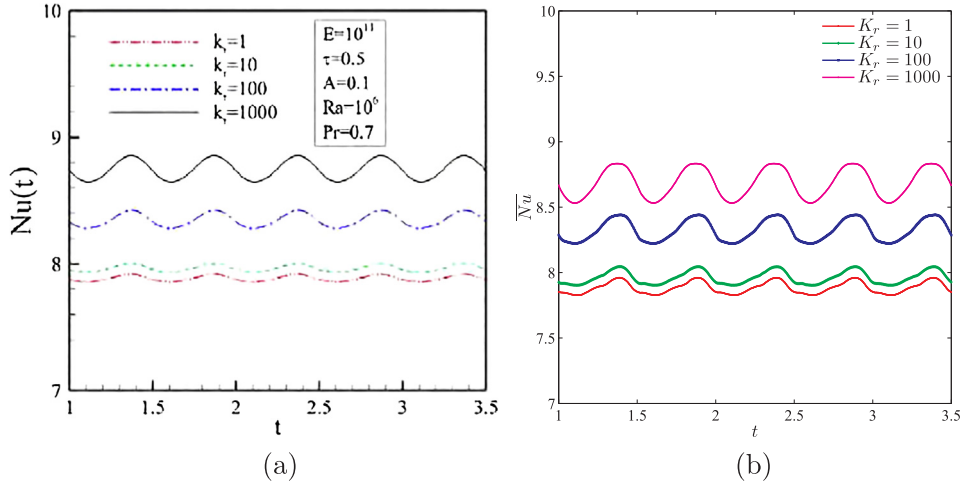

Fig. 7. Comparison of the mean Nusselt number with dimensionless time obtained from present numerical simulation with the numerical results of Ghalambaz et al. [22] for different values of K_r at $Ra = 10^6$, $K_r = 10$, $E = 10^{11}$, $A = 0.1$, $H = 1$, $\phi = 0$ and Pr = 0.7.

transfer in a non-rectangular geometry is consider to be more difficult than that of square/rectangular cavities due to the presence of sloping walls. Generally, the mesh nodes do not lie along the sloping walls, and consequently, from a programming and computational point of view, the efforts required for generating the flow characteristics rise significantly [28]. An excellent review on the natural convection heat transfer in particular case of the parallelogrammic ((oblique) cavities and for various engineering applications was reported by Baïri et al. [29]. Hyun and Choi [30] studied numerically the flow circulations and the temperature fields during the unsteady regime within parallelogram (oblique) cavity for high Rayleigh number (10^7) using the finite difference method. Their study considered several values of the inclination angles of the sloping walls, aspect ratios and Prandtl numbers. The investigation showed that the flow and temperature fields depended on the inclination angle of the sloping walls and the aspect ratio. Using the finite difference method, Han and Hyun [31] studied numerically the buoyant convection heat transfer in a parallelogrammic (oblique) cavity filled with a porous medium, where the horizontal walls of the enclosure are heated to different temperature and the inclined sidewalls wall are kept adiabatic. The results indicated that the heat transfer rate is clearly enhanced by increasing the inclination angle of the sloping walls of the cavity. The work related to the thermal regulation of electronic devices was presented by Baïri et al. [32]. They considered the natural convection in parallelogrammic (oblique) cavities filled with air. They studied experimentally and numerically by the finite volume method the steady and unsteady regimes for high Rayleigh numbers (10^5-10^9) and for different inclination angles (0, 30, 60). They showed that the strong enhancement of the heat transfer clearly appeared for the case of square cavity in the transient regime. Ghalambaz et al. [33] considered a numerical study on the natural convection in a parallelogrammic porous cavity filled with a nanofluid. They reported that increasing the inclination angle of the sloping wall to the positive values tended to enhance the heat transfer rate. While, Nayak et al. [34] presented a Numerical investigation on mixed convection and entropy generation of in a differentially heated skewed cavity filled with nanofluid and they discovered that the flow field, heat transfer and entropy generation were clearly affected by the skew angle. Alsabery et al. [35] studied the unsteady natural convection heat transfer porous oblique cavity saturated with nanofluid using local thermal non-equilibrium model. They found that the increasing of the strength of the flow circulation with the rising of the inclination angle to the positive direction. Alsabery et al. [36] reported a numerical investigation on the effects of viscous dissipation, radiation and constant heat flux on MHD convective heat transfer in an oblique porous cavity. Where they described the enhancement of the heat transfer rate as the inclination angle of the sloping walls increased. Recently, Das et al. [37] reported an excellent review on the natural convection heat transfer within non-rectangular cavities.

According to the above mentioned studies and to the authors' best knowledge, no studies have been reported on the problem of fluid-structure interaction in natural convection heat transfer in an oblique cavity with a flexible oscillating fin. Thus, the authors of the present study believe that this work is valuable. Therefore, following the study of Ghalambaz et al. [22], the present study aims to analyze the FSI in natural convection heat transfer in an oblique cavity with a flexible oscillating fin and partial heating. Two different heating sources are placed in various locations within the oblique cavity. Such a work can be used for improving the thermal performance and the heat transfer enhancement in some engineering instruments, solar-energy systems and nuclear energy systems. In addition, the geometry of oblique cavity has found important applications in shielding of electronic components. The electronic component with surface generated heat flux can be mounted over a portion of the side wall of the oblique cavity while the geometry of the enclosure can be utilized as an extended surface heat sink. The oblique enclosure geometry has also found applications in building of semi-honeycomb metal structures. When a metal structure, covered with a thick insulated mesh cover, is exposed to a laser heat flux, solar radiation or a high convective hot area, the walls of the oblique shape cavity are subject to partial heating boundary conditions.

2. Mathematical formulation

Two-dimensional transient natural convection in an oblique cavity with side L and inclination angle of the sloping wall ϕ is considered in this study as presented in Fig. 1. The right inclined wall of the cavity is maintained at a constant cold temperature T_c and the left inclined wall is heated partially with length h, while the remainder of the left wall is adiabatic. The horizontal walls are thermally insulated except the part that attached the elastic of the bottom wall which is maintained at a constant hot temperature T_h. A hot elastic thin fin with a length d and a thickness b is attached in a cantilever form on the mid height of the bottom horizontal wall. The free end of the elastic fin oscillates sinusoidally as presented in the following equation:

$$x = a \sin\left(\frac{2\pi t^*}{\tau^*}\right), \tag{1}$$

where x is the horizontal position of the free end of the fin, t^* is the dimensional time, a is the dimensional oscillation amplitude and τ^* presents the dimensional oscillation period. The oscillation frequency can be defined as $\lambda^* = \frac{1}{\tau^*}$. The fluid within the oblique cavity is

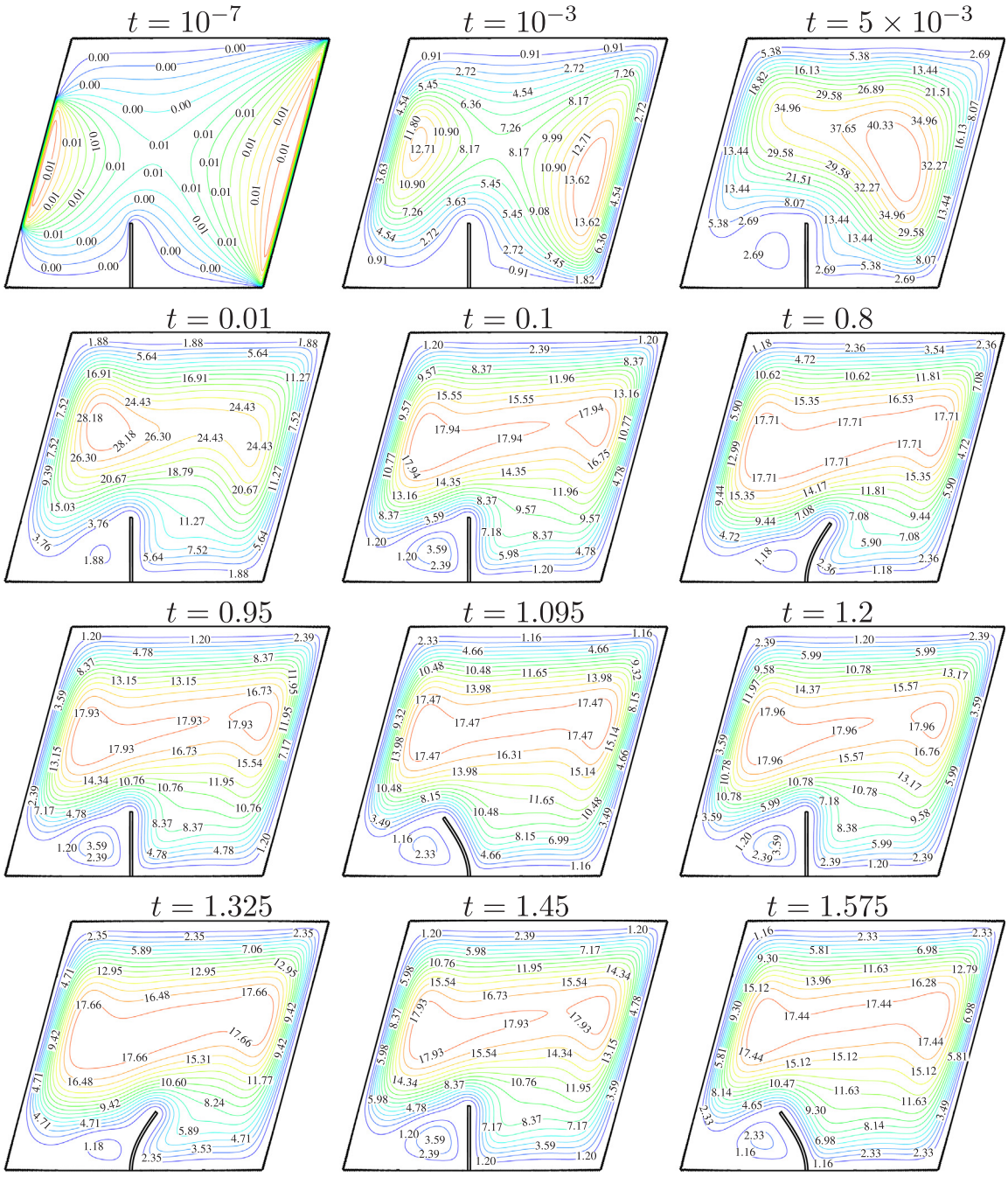

Fig. 8. Streamlines for various dimensionless times (t) for $K_r = 10$, $E = 10^{11}$, $A = 0.1$, $H = 0.5$ and $\phi = 30$.

considered to be laminar, incompressible, and Newtonian. The fluid thermo-physical properties are independent of the temperature variation and the Boussinesq approximation for density is applicable. The dimensional governing equations for the geometrically nonlinear elasto-dynamic structural displacement and energy of the fin can be written as [22]:

$$\rho_s \frac{d^2 d_s^*}{dt^{*2}} - \nabla\sigma^* = F_v^*, \tag{2}$$

$$\frac{\partial T}{\partial t^*} = \alpha_s \nabla^2 T. \tag{3}$$

The dimensional governing equations of conservation of mass, momentum and energy in the Arbitrary Lagrangian-Eulerian (ALE) formulation are written as follows [22]:

$$\nabla \cdot u^* = 0, \tag{4}$$

$$\frac{\partial u^*}{\partial t^*} + \left(u^* - w^*\right)\cdot \nabla\, u = -\frac{1}{\rho_f}\nabla P^* + \nu_f \nabla^2 u^* + \beta g (T - T_c), \tag{5}$$

$$\frac{\partial T}{\partial t^*} + \left(u^* - w^*\right)\cdot \nabla T = \alpha_f \nabla^2 T, \tag{6}$$

here σ^* presents the stress tensor, d_s^* shows the dimensional solid displacement vector, F_v^* is the dimensional applied body force, u^* presents the fluid velocity vector, w^* shows the dimensional moving coordinate velocity, P^* is the dimensional fluid pressure while T presents the dimensional fluid/solid temperature. The fluid and solid densities are denoted by ρ_f and ρ_s, respectively. α_f and α_s are represent the thermal diffusivity of the fluid and solid, respectively. ν_f shows the kinematic

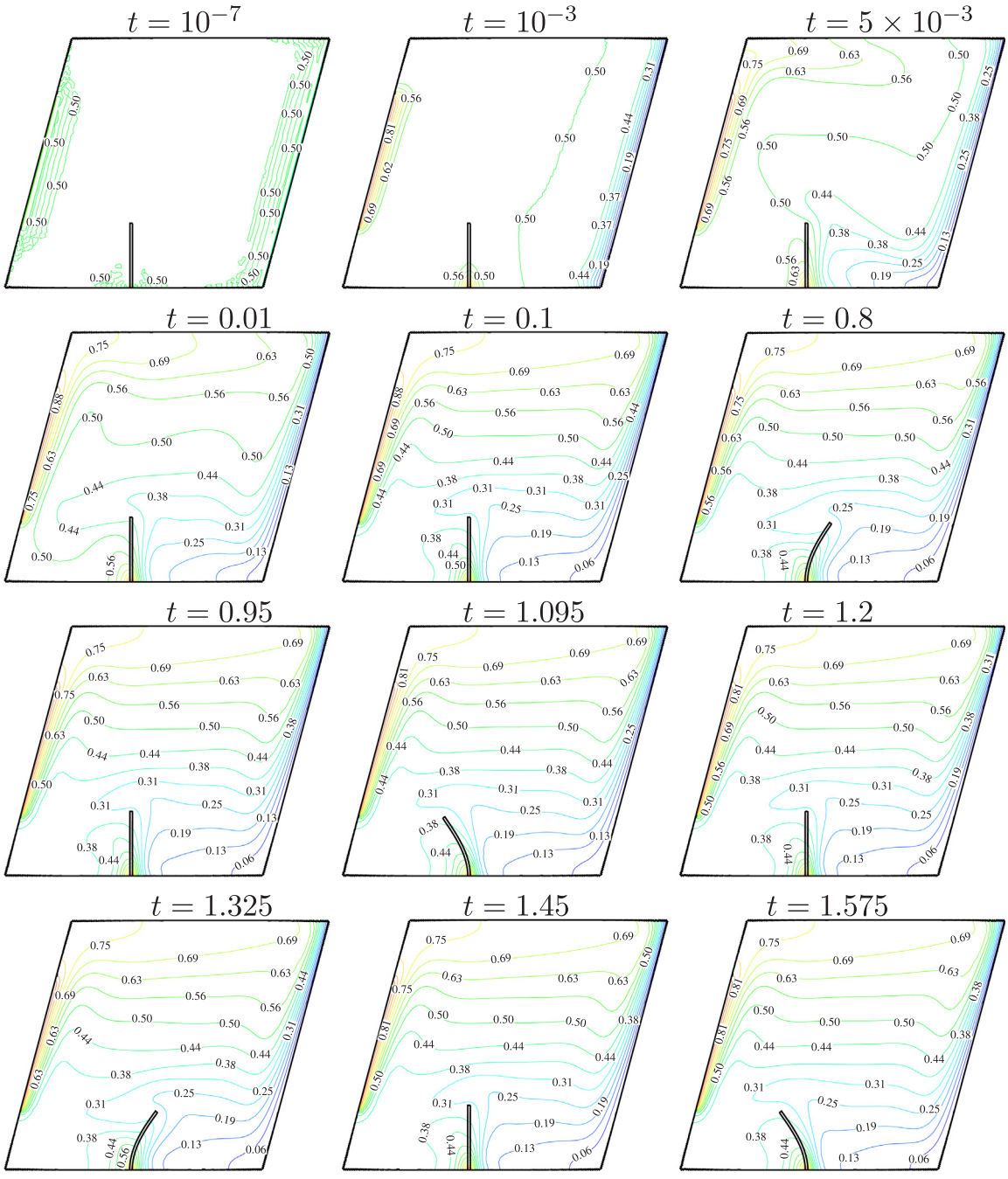

Fig. 9. Isotherms for various dimensionless times (t) for $K_r = 10$, $E = 10^{11}$, $A = 0.1$, $H = 0.5$ and $\phi = 30$.

viscosity of the fluid, g is the acceleration due to gravity, and β presents volumetric thermal expansion coefficient.

Considering the fin as linearly elastic, and taking into account the nonlinear geometry effects, the stress tensor σ is written as:

$$\sigma = J^{-1}\mathrm{FSF}^{T}, \tag{7}$$

where F= $(1 + \nabla d_s^*)$ and $J = \det.(F)$. The second Piola-Kirchhoff stress tensor S is related to strains ε as

$$S = C{:}\,(\varepsilon) \quad \varepsilon = \frac{1}{2}(\nabla d_s^* + \nabla d_s^{*T} + \nabla d_s^{*T}{\cdot}\nabla d_s^*), \tag{8}$$

where $C = C(E^*, \nu)$. The dimensional boundary conditions for the fluid-solid interaction at the fin surfaces are continuity of kinematic forces and dynamic movements. The no-slip boundary condition is consider for the fluid at the solid interface as:

$$\frac{\partial d_s^*}{\partial t^*} = u^* \quad \text{and } \sigma^*{\cdot}\,n = -P^* + \mu_f \nabla u^*. \tag{9}$$

The energy balance equation at the interface of the fluid-solid interaction can be written as:

$$k_f \frac{\partial T}{\partial n} = k_s \frac{\partial T}{\partial n}. \tag{10}$$

The fin clamps with the condition $\frac{\partial d_s^*}{\partial t^*} = 0$. The pressure constraint is assumed as follows:

$$P^* = 0. \tag{11}$$

We now introduce the following dimensionless variables:

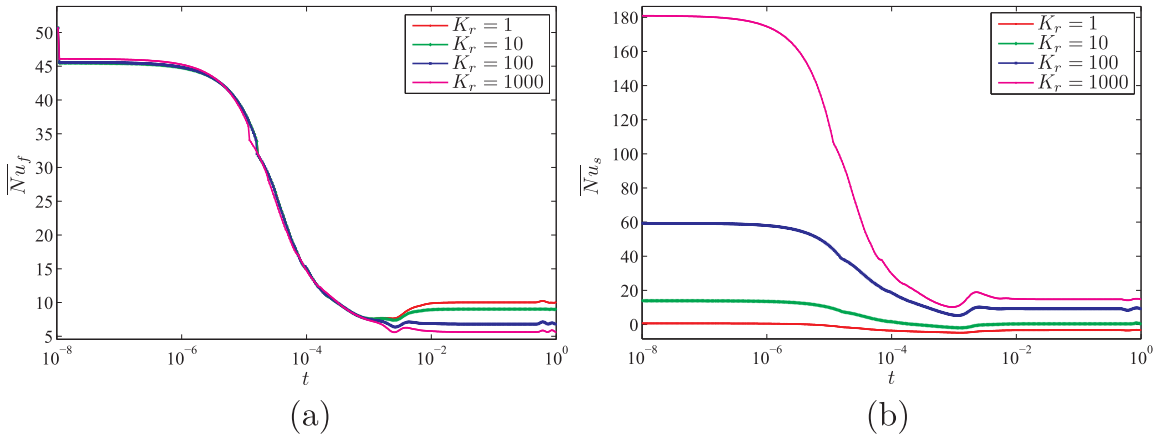

Fig. 10. Variation of the unsteady average Nusselt number on (a) inclined left wall and (b) solid fin with t for different K_r at $E = 10^{11}$, $A = 0.1$, $H = 0.5$ and $\phi = 30$.

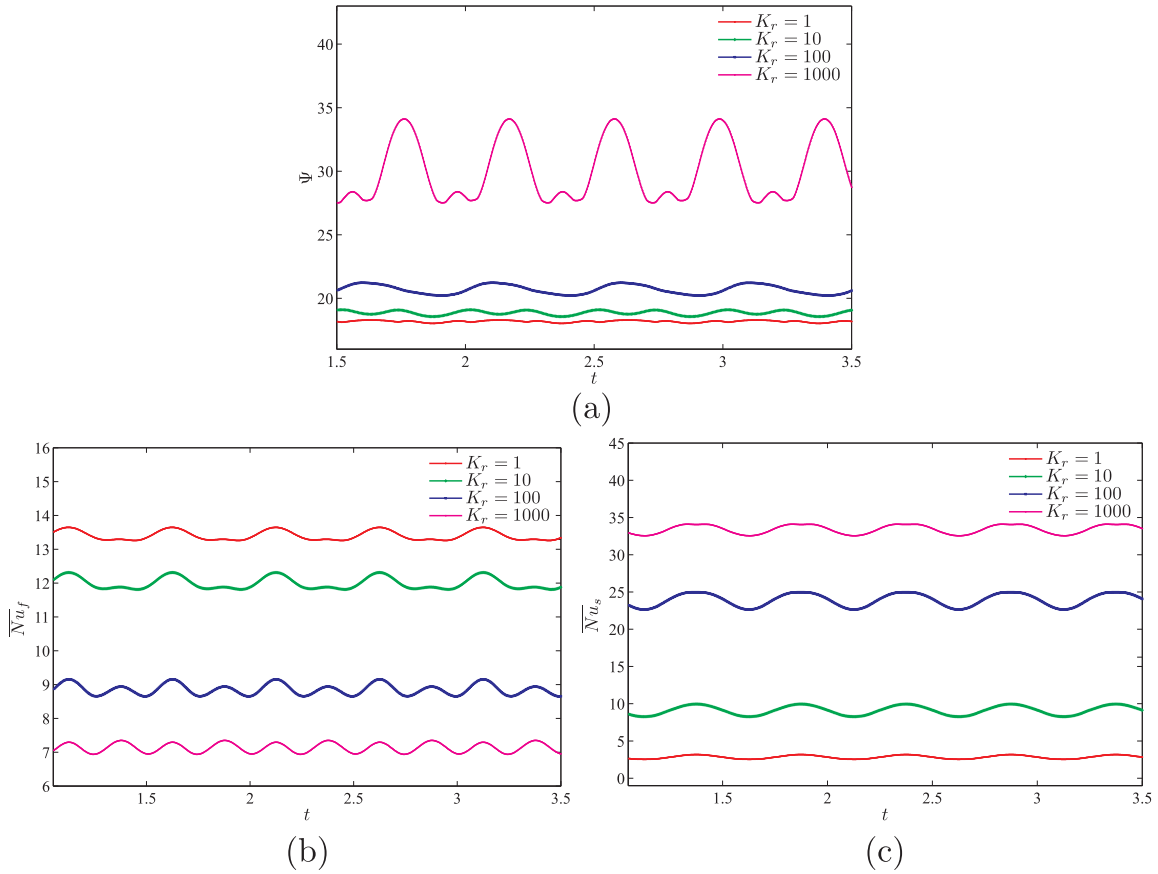

Fig. 11. Variation of (a) strength of the flow circulation, (b) the average Nusselt number on the inclined left wall and (c) the solid fin with t for different K_r at $E = 10^{11}$, $A = 0.1$, $H = 0.5$ and $\phi = 30$.

$$X = \frac{x}{L}, \quad Y = \frac{y}{L}, \quad \left(A, H, B\right) = \frac{(a, h, b)}{L}, \quad \left(\mathrm{u}, \mathrm{v}\right) = \frac{(\mathrm{u}^*, \mathrm{v}^*)L}{\alpha_f},$$
$$\mathrm{w} = \frac{\mathrm{w}^* L}{\alpha_f}, \quad \theta = \frac{T - T_c}{T_h - T_c}, \quad \mathrm{d}_s = \frac{\mathrm{d}_s^*}{L}, \quad \sigma = \frac{\sigma^*}{E^*}, \quad t = \frac{t^* \alpha_f}{L^2},$$
$$\tau = \frac{\tau^* \alpha_f}{L^2}, \quad P = \frac{L^2}{\rho_f \alpha_f^2} P^*, \quad \mathrm{F}_\mathrm{v}^* = \rho_s \cdot g. \tag{12}$$

In addition, the dimensionless stream function (Ψ) is defined to describe the fluid motion and can be evaluated as the following:

$$\mathrm{u} = \frac{\partial \Psi}{\partial Y}, \quad \mathrm{v} = -\frac{\partial \Psi}{\partial X}. \tag{13}$$

This then yields the dimensionless governing equations are:

$$\frac{1}{\rho_r} \frac{d^2 \mathrm{d}_s}{dt^2} - E \cdot \nabla \sigma = E \cdot \mathrm{F}_\mathrm{v}, \tag{14}$$

$$\frac{\partial \theta}{\partial t} = \alpha_r \cdot \nabla^2 \theta, \tag{15}$$

$$\nabla \cdot \mathrm{u} = 0, \tag{16}$$

$$\frac{\partial \mathrm{u}}{\partial t} + \left(\mathrm{u} - \mathrm{w}\right) \cdot \nabla \mathrm{u} = -\nabla P + \mathrm{Pr} \cdot \nabla^2 \mathrm{u} + \mathrm{Pr} \cdot Ra \cdot \theta \cdot \hat{e}_j, \tag{17}$$

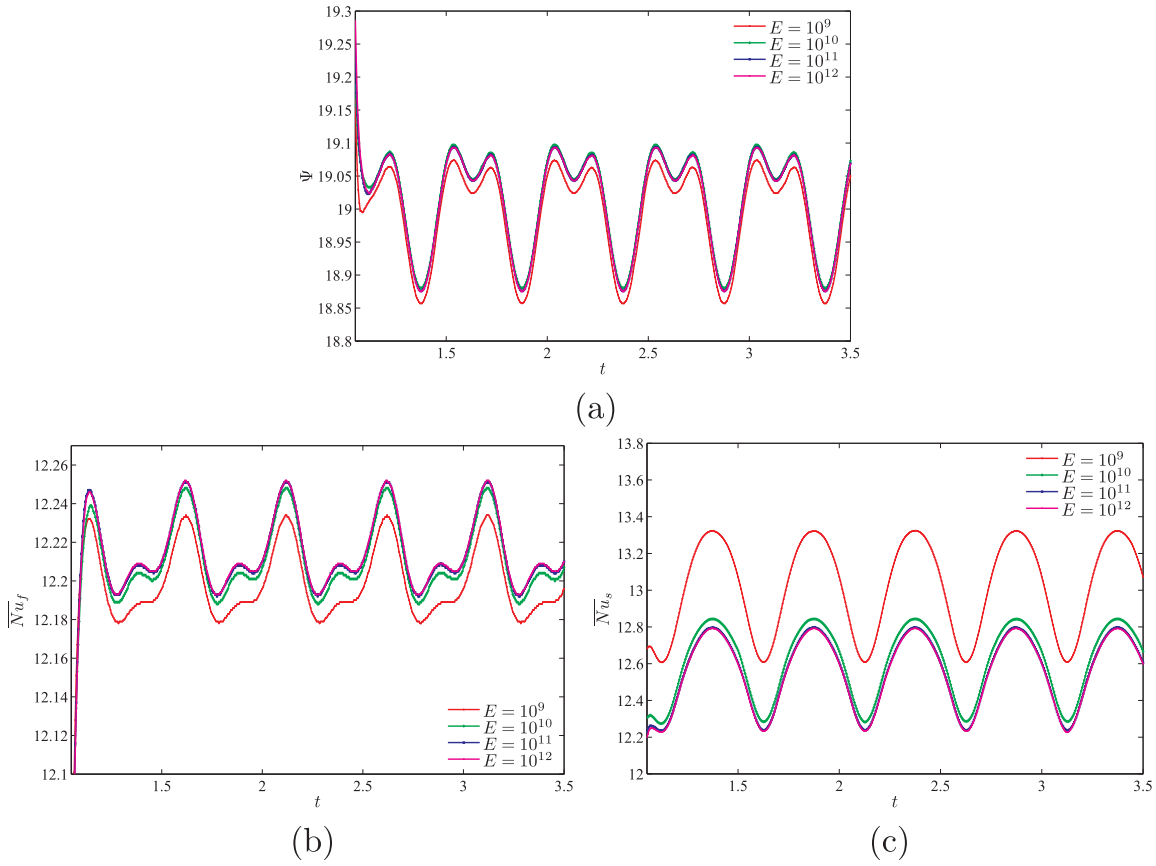

Fig. 12. Variation of (a) strength of the flow circulation, (b) the average Nusselt number on the inclined left wall and (c) the solid fin with t for different E at $K_r = 10$, $A = 0.1$, $H = 0.5$ and $\phi = 30$.

$$\frac{\partial\theta}{\partial t} + \left(\mathrm{u}-\mathrm{w}\right)\cdot\nabla\theta = \nabla^2\theta, \tag{18}$$

where $Ra = g\rho_f\beta(T_h-T_c)L^3/(\mu_f\alpha_f)$ is the Rayleigh number, $\mathrm{Pr} = \nu_f/\alpha_f$ is the Prandtl number, $E = E^*L^2/\rho_f\alpha_f^2$ is the flexibility parameter, $\mathrm{F_v} = (\rho_f-\rho_s)Lg/E^*$ is the body force parameter, $\rho_r = \rho_f/\rho_s$, $\alpha_r = \alpha_f/\alpha_s$ are the thermal diffusivity ratio and the density ratio parameter and $\mathrm{F_v}$ denotes the dimensionless body force.

The values of the dimensionless velocity are zero in the solid walls of the oblique cavity. The dimensionless initial and boundary conditions of Eqs. (14)–(18) are:

$$\Psi = 0, \quad \theta = 0.5, \quad \text{on the walls of the cavity} \quad \text{at} \quad t = 0, \tag{19}$$

$$\Psi = 0, \quad \text{on all walls}, \quad t > 0, \tag{20}$$

$$\text{On AD, } \theta = 1, \text{ at } (1-H)/2 \leqslant Y \leqslant (1+H)/2, \tag{21}$$

$$\text{on the adiabatic parts of AD } \frac{\partial\theta}{\partial Y} = 0. \tag{22}$$

$$\text{On BC, } \theta = 0, \tag{23}$$

$$\text{On AB, } \theta = 1, \text{ at } (1-B)/2 \leqslant X \leqslant (1+B)/2, \tag{24}$$

$$\text{On the adiabatic parts of AB, and DC, } \frac{\partial\theta}{\partial X} = 0, \tag{25}$$

$$\left(\frac{\partial\theta}{\partial \mathrm{n}}\right) = K_r\left(\frac{\partial\theta}{\partial \mathrm{n}}\right) \text{ for the solid fin,} \tag{26}$$

where $K_r = k_s/k_f$ is the thermal conductivity ratio. The solid-fluid interaction boundary conditions are also can be written as follows:

$$\frac{\partial \mathrm{d}_s}{\partial t} = u \text{ and } E\cdot\sigma\cdot \mathrm{n} = -P + \mathrm{Pr}\cdot\nabla u. \tag{27}$$

The dimensionless initial temperature at the fluid and the fin is assumed as $\theta = 0.5$. The dimensionless initial velocity is u= 0. For the pressure point constraint, the following dimensionless pressure constraint is also considered:

$$P = 0. \tag{28}$$

The dimensionless tip displacement of the fin is also obtained as:

$$X = A\sin\left(\frac{2\pi t}{\tau}\right). \tag{29}$$

On using the transformation $\xi = X - Y\tan\phi$, $\eta = \frac{Y}{\cos\phi}$ [35], the local Nusselt number at the inclined left hot boundary may now be defined as follows [36]:

$$Nu_f = -\tan\phi\frac{\partial\theta}{\partial\eta} + \frac{1}{\cos\phi}\frac{\partial\theta}{\partial\xi}\bigg|_{\xi=0}, \tag{30}$$

and the local Nusselt number at the basis of the solid fin, which can be written as:

$$Nu_s = -K_r\frac{\partial\theta}{\partial X}\bigg|_{Y=0}. \tag{31}$$

The average Nusselt number at the heated part of the inclined left wall of the cavity can be introduced as [36]:

$$\overline{Nu}_f = \int_{\frac{1-H}{2}}^{\frac{1+H}{2}} Nu_f\,\mathrm{d}\eta, \tag{32}$$

and the average Nusselt number at the basis of the fin can be introduced as:

$$\overline{Nu}_s = \int_{S_1}^{S_2} Nu_s\,\mathrm{d}Y, \tag{33}$$

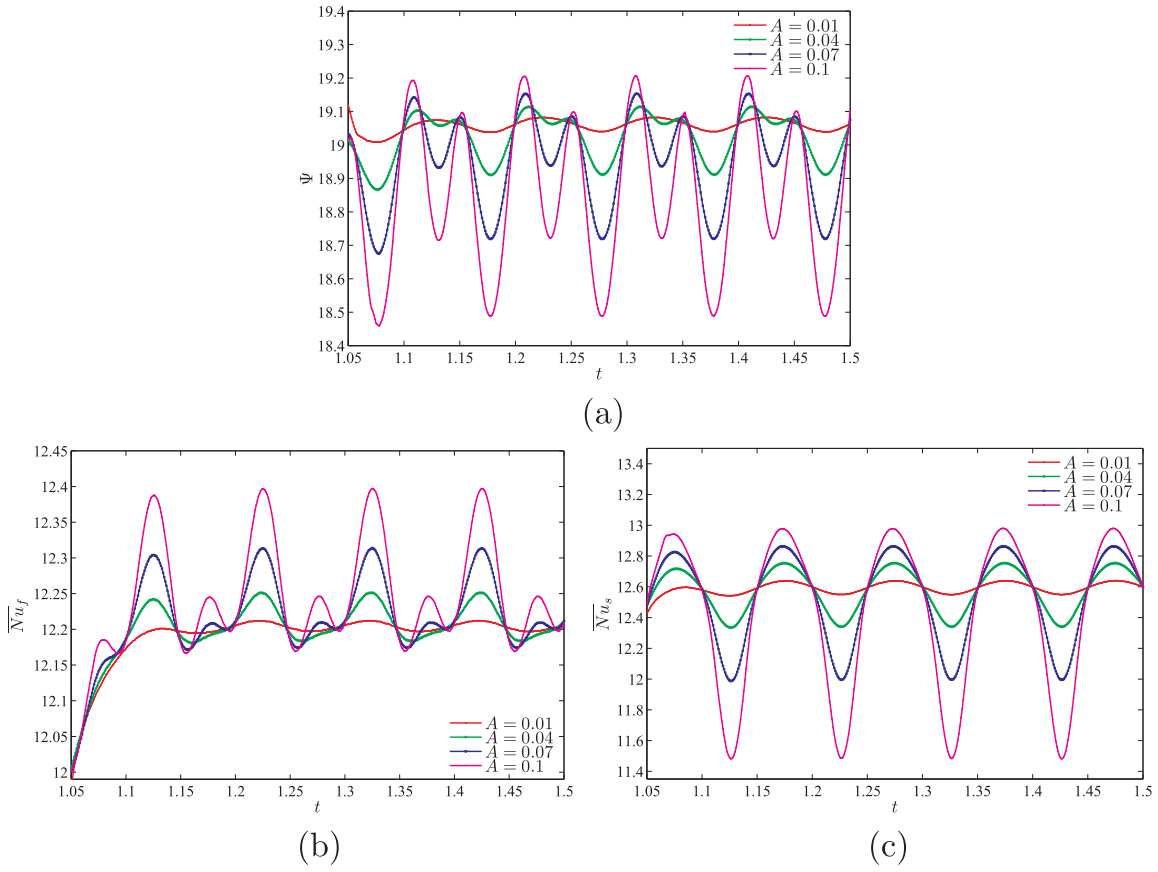

Fig. 13. Variation of (a) strength of the flow circulation, (b) the average Nusselt number on the inclined left wall and (c) the solid fin with t for different A at $K_r = 10$, $E = 10^{11}$, $H = 0.5$ and $\phi = 30$.

where $S_1 = \frac{1}{2} - \frac{b}{2}$ and $S_2 = \frac{1}{2} + \frac{b}{2}$.

3. Numerical method and validation

The dimensionless governing Eqs. (14)–(18) subject to the initial and boundary conditions (19)–(26) are solved numerically by the Galerkin weighted residual finite element method. The computational domain is discretized into triangular elements as shown in Fig. 2. Triangular Lagrange finite elements of different orders are used for each of the flow variables within the computational domain. Residuals for each conservation equation are obtained by substituting the approximations into the governing equations. To simplify the nonlinear terms in the momentum equations, a Newton-Raphson iteration algorithm was used. The convergence of the solution is assumed when the relative error for each of the variables satisfies the following convergence criterion:

$$\left|\frac{\Gamma^{i+1}-\Gamma^{i}}{\Gamma^{i+1}}\right| \leqslant \eta,$$

where i represents the iteration number and η is the convergence criterion. In this study, the convergence criterion was set at $\eta = 10^{-6}$.

In the present study, the period of the fin oscillation, is adopted as $\tau = 0.1$. The results are obtained for $\tau/100$ or $\Delta t = 0.001$. However, for the calculation an automatic time scheme is utilized. The Backward Differentiation Formula (BDF) with free time steps is employed as an implicit time step method. The maximum and minimum order of BDF are set as 1 and 2, respectively. The BDF solver interpolates between the accuracy of the previous time steps, and automatically determines the adequate computational time steps to ensure the accuracy and time convergence of the calculations. Details of BDF scheme can be found in [38,39]. Fig. 3 shows the flowchart of the utilized numerical code. As seen, the heat, flow, elastic structure, and the grid motion are solved iteratively. Then, the convergence is monitored until the convergence in the time step is reached. After that, BDF automatic time step solver is updated and an adequate time step is selected, and calculations are repeated for a new time step.

We have employed grids with various sizes to ensure that the present numerical solution is independent on the grid size for the numerical domain, we have used different grid sizes to calculate the average Nusselt number on the inclined left wall and the average Nusselt number on the solid fin for the steady case ($t = 3.5$), $Ra = 10^6$, $K_r = 10$, $E = 10^{11}$, $A = 0.1$, $H = 0.5$ and $\phi = 30$. Based on the results examined in Fig. 4, insignificant differences surrounding the G6 grids and above were observed. Therefore, the G6 uniform grid is used to perform all the computations in this paper to solve similar problems as in this subsection.

For the validation of the present work, the results of present study have been compared with the experimental results reported by Nishimura et al. [40] and the numerical results described by Churchill [41] for natural convection in a cavity with temperature difference at its side walls. The results are depicted in Fig. 5 when Pr = 6.0. As seen, there is a good agreement between the results of both studies. Also, the current results are compared with the earlier published works of Ghalambaz et al. [22] for the case of natural convection heat transfer over a horizontal flexible oscillating fin within a square cavity differently heated vertical walls and filled with air at $Ra = 10^6$, $K_r = 10$, $E = 10^{11}$, $A = 0.1$, $H = 1$, $\phi = 0$ and Pr = 0.7, as shown in Fig. 6. In addition, another validation is achieved by comparing the average Nusselt number with dimensionless time of the present work with the numerical results of Ghalambaz et al. [22] for different values of K_r at $Ra = 10^6$, $E = 10^{11}$, $A = 0.1$, $H = 1$, $\phi = 0$ and Pr = 0.7, as displayed in Fig. 7. Based on these validations, it is found that the present result is in a very good agreement with the results of

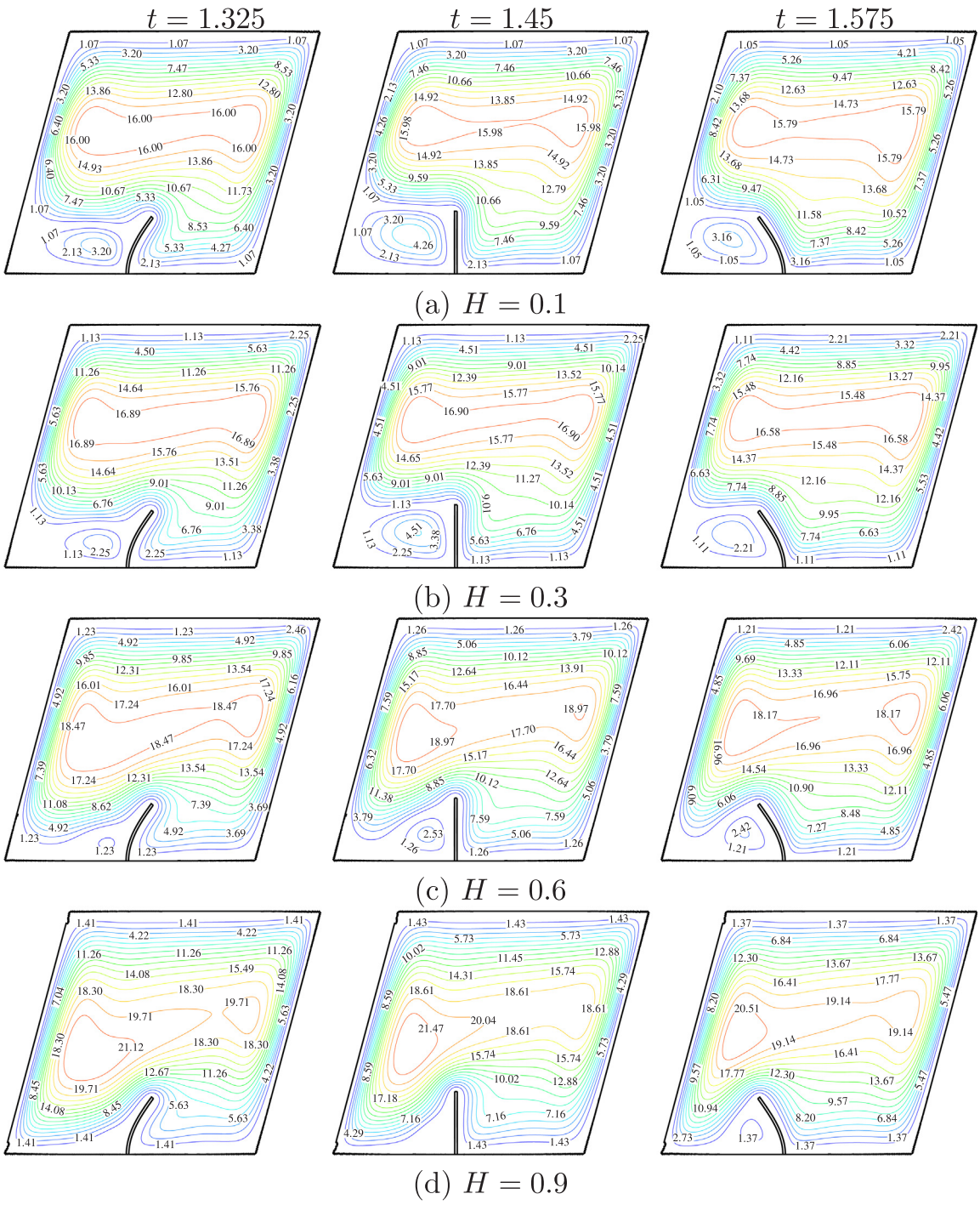

Fig. 14. Streamlines for various dimensionless times (t) and dimensionless length of the heat source (H) for $K_r = 10$, $E = 10^{11}$, $A = 0.1$, $\phi = 30$.

the previously published works.

4. Results and discussion

We present numerical results for the streamlines and isotherms with various dimensionless times ($10^{-8} \leqslant t \leq 3.5$), thermal conductivity ratio between the heat-conducting fin and working medium ($1 \leqslant K_r \leq 1000$), dimensionless Young's modulus ($10^9 \leqslant E \leq 10^{12}$), amplitude of the oscillating fin ($0.01 \leqslant A \leqslant 0.1$), dimensionless length of the heater ($0.1 \leqslant H \leq 0.9$), and inclination angle of the sloping wall ($-45 \leqslant \phi \leqslant 45$). The values of the Rayleigh number, dimensionless fin thickness and Prandtl number are fixed at $Ra = 10^6$, $B = 0.01$ and Pr = 6.2, respectively.

Figs. 8 and 9 show an evolution of the streamlines and isotherms for $K_r = 10$, $E = 10^{11}$, $A = 0.1$, $H = 0.5$ and $\phi = 30$. The initial time level ($t = 10^{-7}$) characterizes a formation of low intensive convective flows near the left wall heat source and the right cold wall, where one can find a great temperature difference taking into account the used non-dimensionalization. A further time moment ($t = 10^{-3}$) reflects more intensive circulation with heating near the left heat source and cooling close to the right cold wall. At the same time, a presence of the local heater leads to an appearance of the convective cell core near the upper border of the heater, while near the right wall the convective cell core displaces to the bottom wall. Such behavior can be explained by the

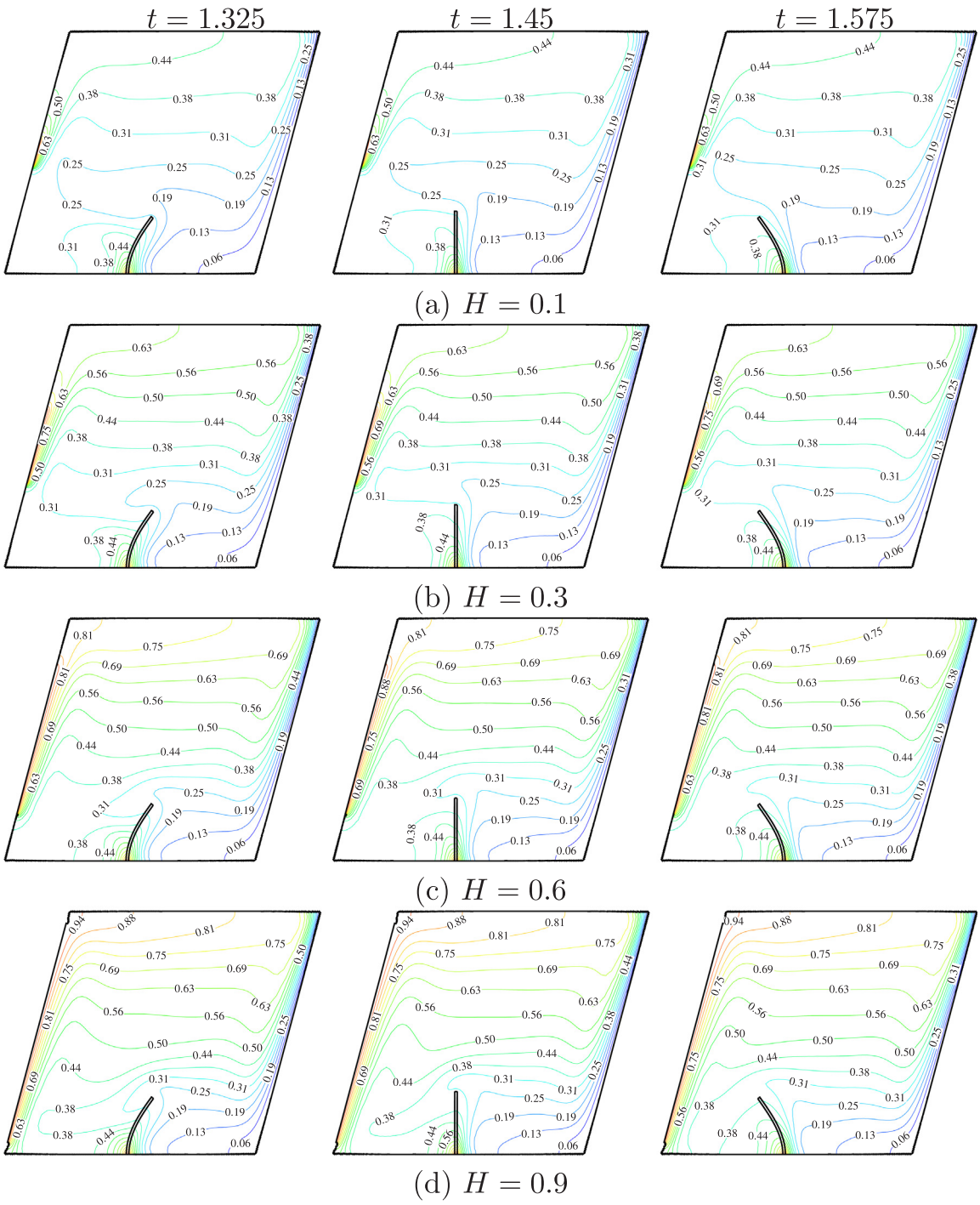

Fig. 15. Isotherms for various dimensionless times (t) and dimensionless length of the heat source (H) for $K_r = 10$, $E = 10^{11}$, $A = 0.1$, $\phi = 30$.

directions of major flows near the hot and cold elements taking into account the dependence of the density on the temperature. It should be noted that the flexible heat-conducting fin is heated from the bottom and one can find in Fig. 9 for $t = 10^{-3}$ a distribution of high temperature from this point. In the case of $t = 5{\cdot}10^{-3}$ two convective cells are combined with a formation of major one near the right cold wall. This convective cell has maximum value of the circulation intensity in comparison with other time moments. Isotherms for this time moment illustrate a formation of descending thermal boundary layer near the right cold wall and ascending thermal boundary layer near left local heater with more essential heating of the flexible heat-conducting fin. The latter leads to an appearance of minor circulation to the left of this fin. Further growth of time reflects an attenuation of convective flow due to the homogenization of temperature inside the cavity with a reduction of the temperature difference. For $5{\cdot}10^{-3} \leqslant t \leq 0.1$ the convective cell core displaces to the left wall heater with an intensification of recirculation near the flexible heat-conducting fin. At the same time, the isotherms illustrate a formation of a temperature stratification core for $t = 0.1$. The considered time moments from 10^{-7} till 0.1 reflect an evolution of the fluid flow and heat transfer where the flexible heat-conducting fin is motionless. In the case of $t = 0.8$, one can find a displacement of the upper fin part to the right side due to strong recirculation near this fin presented for $t = 0.1$. Further growth of time characterizes an oscillation of this heat-conducting fin that changes the

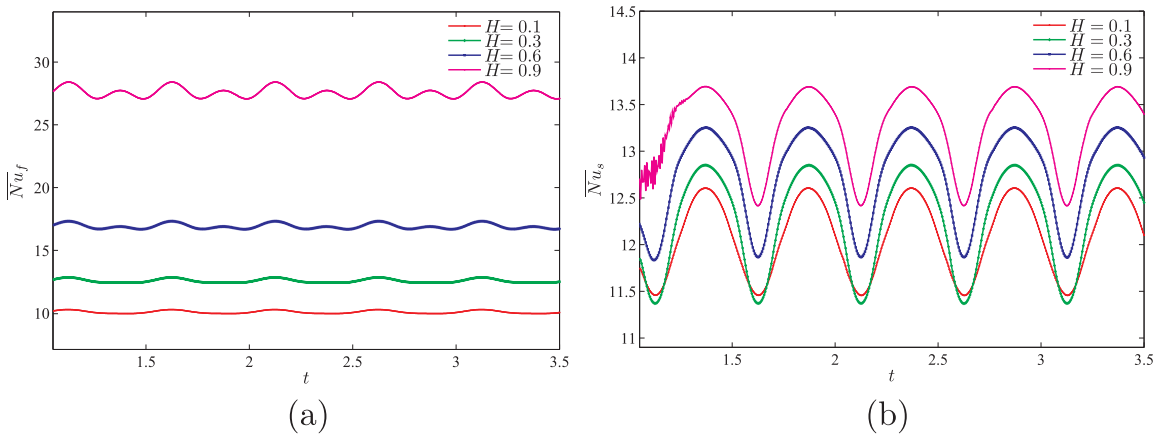

Fig. 16. Variation of the average Nusselt number on (a) the inclined left wall and (b) the solid fin with t for different H at $K_r = 10$, $E = 10^{11}$, $A = 0.1$ and $\phi = 30$.

fluid structure near this fin, while the major convective cell core also has weak changes. It should be noted that the temperature field also reflects a modification of the temperature near and inside this fin. It seems that an origin of fin oscillation reflects a formation of periodical temperature field and fluid structures close to this fin.

Fig. 10 demonstrates the average Nusselt number behavior at the heat source (Fig. 10a) and at the fin surface (Fig. 10b) at the initial time level where $10^{-8} \leqslant t \leqslant 1.0$ for different values of the thermal conductivity ratio. It is worth noting that for $10^{-8} \leqslant t \leqslant 10^{-6}$ the average Nusselt numbers are constant which reflects the development of heat conduction, while for $10^{-6} \leqslant t \leqslant 10^{-3}$ the average Nusselt numbers decrease due to the domination of heat conduction where the temperature difference reduces due to heating of the domain near the left wall heater and the fin surface. Further convective heat transfer develops and one can find a weak augmentation of the average Nusselt numbers with further oscillations due to the oscillations of the flexible fin. A growth of the thermal conductivity ratio due to an increase in the solid fin thermal conductivity, illustrates a rise of the average Nusselt number at the fin surface during the considered initial time level. Moreover, for $10^{-8} \leqslant t \leqslant 10^{-5}$ differences for $\overline{Nu}_s$ at different K_r are large due to the heat conduction domination, for $t \geqslant 10^{-5}$ these differences are reduced. At the same time, for the left wall heater $\overline{Nu}_f$ does not depend on K_r for $t < 10^{-3}$, while for $t > 10^{-3}$ a growth of the thermal conductivity ratio leads to a diminution of the average Nusselt number at the heater element. Such a behavior can be explained by more essential heating of the flexible fin that leads to a reduction of the temperature gradient near the left wall heat source.

The periodicity behavior of the fluid flow rate, average Nusselt numbers at the heater surface and the fin surface is presented in Fig. 11 for different values of the thermal conductivity ratio. As has been mentioned above, a growth of K_r leads to both a rise of $\overline{Nu}_s$ (Fig. 11c) due to a formation of high temperature gradient between the hot fin surface and cold right wall, and a reduction of $\overline{Nu}_f$ (Fig. 11b). The reason for the latter behavior was described above. At the same time, the fluid flow intensity increases with K_r (Fig. 11a). It is interesting to note that the oscillations amplitude and frequency for the fluid flow rate increase with the thermal conductivity ratio. The oscillations frequency for the average Nusselt numbers rises also with K_r. It seems that the following growth of the dimensionless time results in a reduction of the oscillations frequency for the average Nusselt at the left wall heater (Fig. 11b).

Fig. 12 shows the effect of the dimensionless Young's modulus on the fluid flow rate and the average Nusselt numbers at the heater surface and the fin surface. For the case of fluid flow rate, a growth of the dimensionless Young's modulus leads to the convective flow intensification for $10^9 \leqslant E \leq 10^{10}$, while for $10^{10} \leqslant E \leq 10^{12}$ one can find a weak attenuation of the convective flow. Such a behavior can be explained by the effect of the fin form on the convective flow and fluid flow structure. It should be noted that the Young's modulus characterizes a stiffness of the considered solid fin and low values reflect an opportunity to have essentially a curved fin. In the case of $\overline{Nu}_f$, a growth of E leads to a rise of the average Nusselt number. Such behavior can be explained by a more stable convective flow due to a presence of a stiff element. At the same time, $\overline{Nu}_s$ decreases with the dimensionless Young's modulus due to a more stable convective flow near the fin and low temperature gradient in this zone.

The effect of the oscillation amplitude on the considered integral parameters is demonstrated in Fig. 13. A growth of the oscillation amplitude for the free end of the elastic fin leads to a growth of the amplitude for the fluid flow rate and heat transfer rates, while the time averaging of the fluid flow rate and the average Nusselt number at the fin surface leads to a reduction of these values with A. At the same time, the time averaging of the average Nusselt number at the heater surface increases with the oscillation amplitude. Fig. 13(b) shows that there are two types of fluctuations of the Nusselt number at the inclined left wall during each oscillation period, $\tau = 0.1$. There is fluctuation with high amplitude and a fluctuation with low amplitude. The high amplitude fluctuation corresponds to the motion of the fin toward the left wall, and the low amplitude one corresponds to the motion of the fin in a direction away from the wall. When the fin moves toward the wall, it pushes the flow toward the element and increases the convective heat transfer. When, the fin moves in a direction away from the wall, it induces two opposite convection mechanisms. The motion of the fin away from the wall tends to induce a flow current opposite to the natural convection circulation flow. The deformed shape of the fin would reduce the pressure drop and flow resistance in a natural convection circulation flow. Therefore, when the fin moves away from the wall, small fluctuations which are the results of these two mechanisms can be seen for the Nusselt number over the wall.

Figs. 14 and 15 present the streamlines and the isotherms for different values of the left wall heater length and for three time moments describing different locations of the free end of oscillation fin. A growth of the heater length leads to the intensification of the major convective vortex, while the minor convective cell attenuates and its size is reduced. A diminution of the minor circulation size can be explained by a growth of the left wall heater surface where one can find a formation of intensive ascending flow, while near the heated fin from each side, an ascending convective flow is also formed. Therefore, at $H = 0.9$ small vortices are formed near the left side of the fin. The temperature fields (Fig. 15) reflect a growth of the heat source surface along the left sloping wall with a strong ascending thermal boundary layer. At the same time, the major convective cell core displaces to the left bottom corner with H, while the intensity of the right one decreases. It is interesting to note that in the case of a vertical fin ($t = 1.45$), the intensity

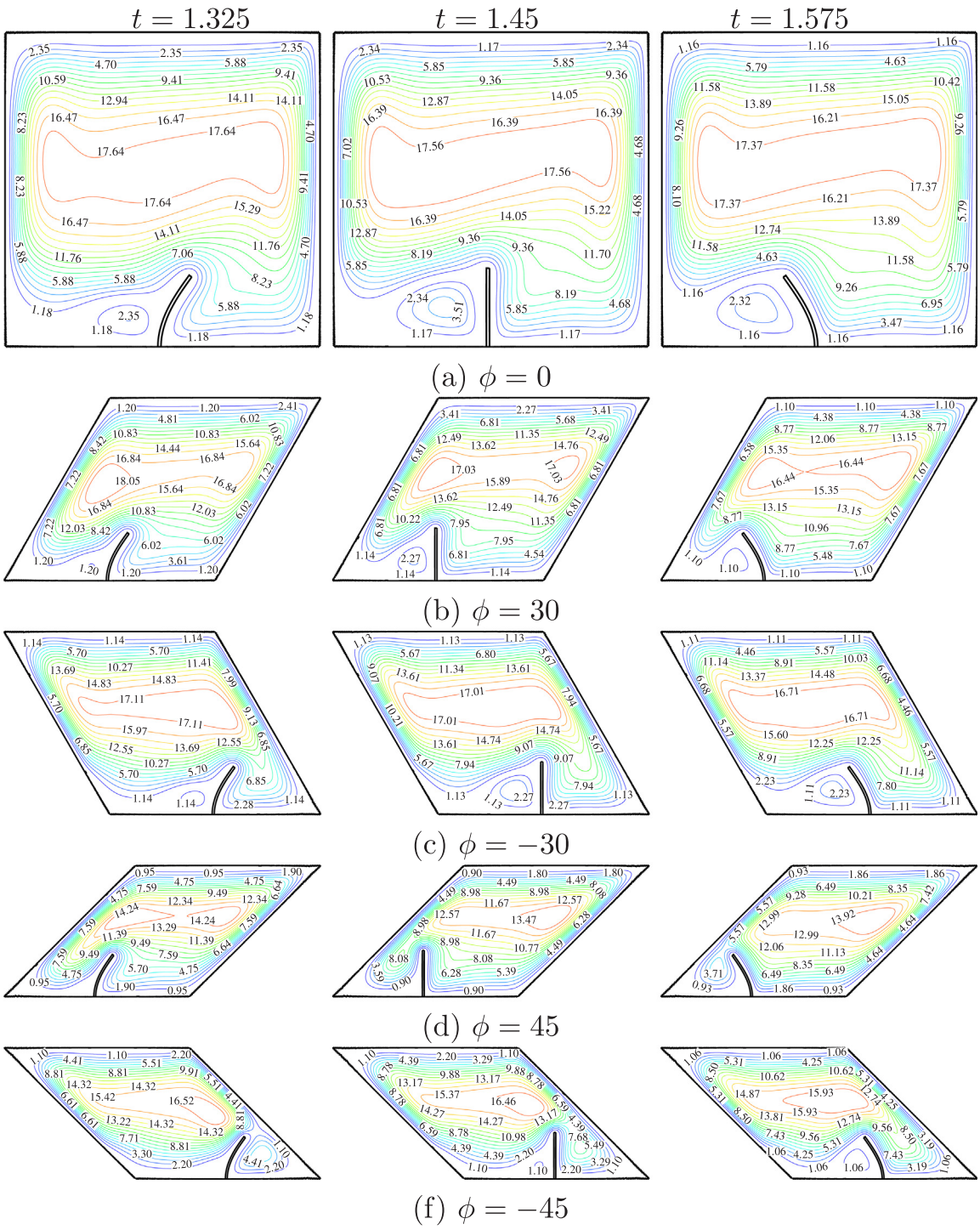

Fig. 17. Streamlines for various dimensionless times (t) and inclination angle of the sloping wall (ϕ) for $K_r = 10$, $E = 10^{11}$, $A = 0.1$ and $H = 0.5$.

of the convective cell near this fin and the major convective cell intensity are maximum in comparison with the other two positions of the fin.

Fig. 16 presents the effect of the left wall heater length on the average Nusselt numbers. A growth of the heater length leads to a rise of the average Nusselt numbers at the heater surface and the fin surface. At the same time, the oscillations amplitude and frequency for the average Nusselt number at the left wall heater surface rise with H, while the oscillations frequency changes weakly.

The effect of the inclination angle of the sloping side walls on the streamlines and the isotherms at $K_r = 10$, $E = 10^{11}$, $A = 0.1$ and $H = 0.5$ is shown in Figs. 17 and 18. A growth of the inclination angle from 0 till 45 results in an attenuation and sizes reduction of the minor circulation near the fin. At the same time, the major fluid flow rate changes non-monotonically. The temperature fields characterize an opportunity to form the confined temperature stratification zone with a quasi-confined vortex when the free end of the fin is near the sloping wall (see the cases of $\phi = \pm 45$, $t = 1.325$ and $t = 1.575$). It is interesting to note that a more intensive circulation inside the central part of the cavity occurs when the upper end of the fin has the right side slope. Such feature does not depend on the inclination angle of the sloping side wall. It is possible to explain this nature by the volume of medium that is under the influence

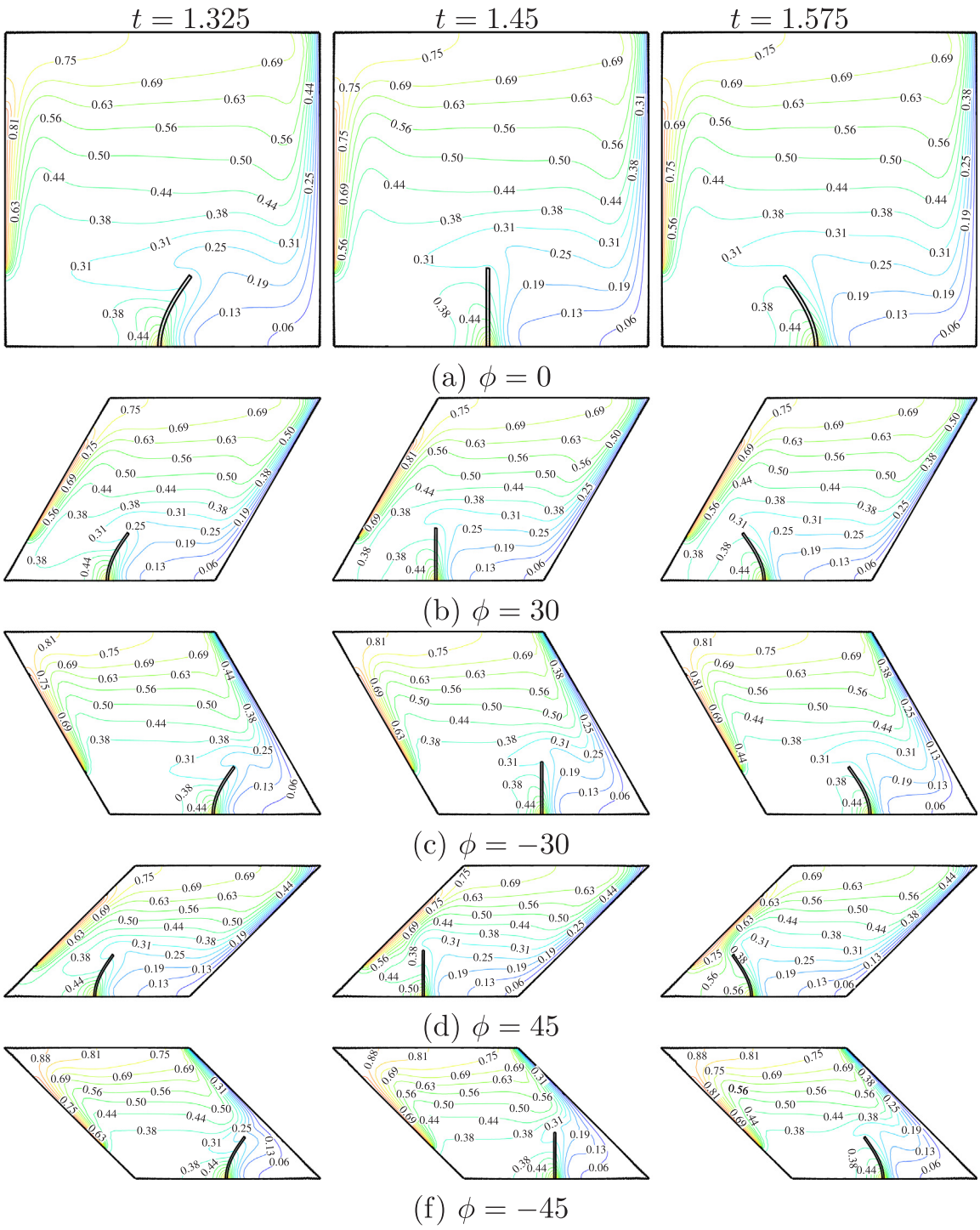

Fig. 18. Isotherms for various dimensionless times (t) and inclination angle of the sloping wall (ϕ) for $K_r = 10$, $E = 10^{11}$, $A = 0.1$, $H = 0.5$.

of the left heater and by a small recirculation formed near the left side of the fin.

Fig. 19 demonstrates the evolution of the average Nusselt numbers at the left wall heater surface and the fin surface at the initial time level for $K_r = 10$, $E = 10^{11}$, $A = 0.1$ and $H = 0.5$ and different values of the sloping wall inclination angle. In the case of $\overline{Nu}_f$, one can find a reduction of this parameter with a growth of the absolute value of the sloping walls inclination angle. A more essential diminution of $\overline{Nu}_f$ with $|\phi|$ occurs for $10^{-8} \leqslant t < 10^{-4}$, while for $t > 10^{-4}$ this reduction is not so significant. In the case of $\overline{Nu}_s$, the influence of ϕ is visible for $10^{-6} \leqslant t < 10^{-4}$ and for this time range a growth of $|\phi|$ leads to a non-monotonic behavior of the average Nusselt number at the solid fin.

Fig. 20 shows the effects of the dimensionless time and the sloping walls inclination angle on the considered average Nusselt numbers for the periodical time level. A growth of the absolute value of ϕ leads to the reduction of the average Nusselt number at the left wall heater surface, while the oscillations amplitude of this average Nusselt number increases. It should be noted that for positive values of the inclination angle the oscillations amplitude is greater in comparison with negative values of the inclination angle. At the same time, a growth of the inclination angle from −45 to 45 characterizes a diminution of the average Nusselt number at the fin surface. Moreover, a more essential

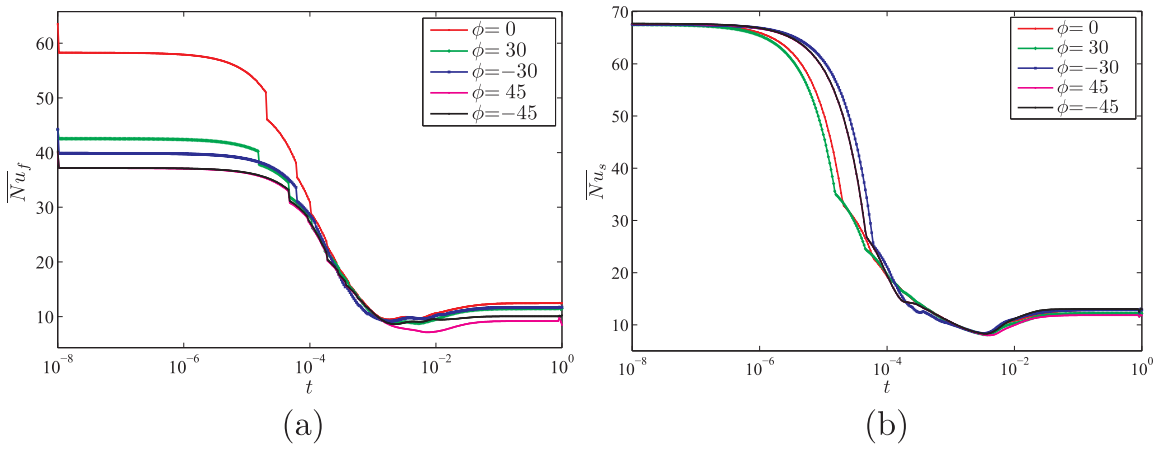

Fig. 19. Variation of the unsteady average Nusselt number on (a) inclined left wall and (b) solid fin with t for different ϕ at $K_r = 10$, $E = 10^{11}$, $A = 0.1$ and $H = 0.5$.

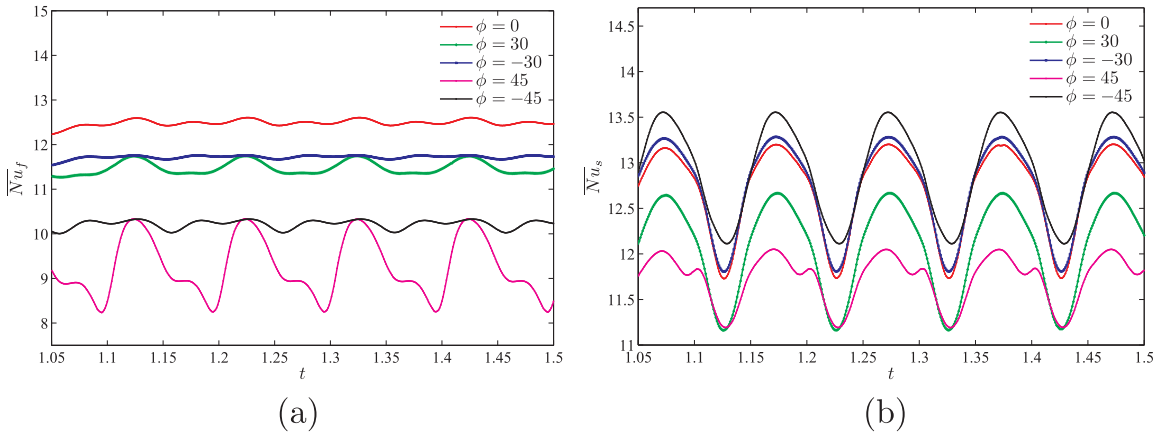

Fig. 20. Variation of the average Nusselt number on (a) the inclined left wall and (b) the solid fin with t for different ϕ at $K_r = 10$, $E = 10^{11}$, $A = 0.1$ and $H = 0.5$.

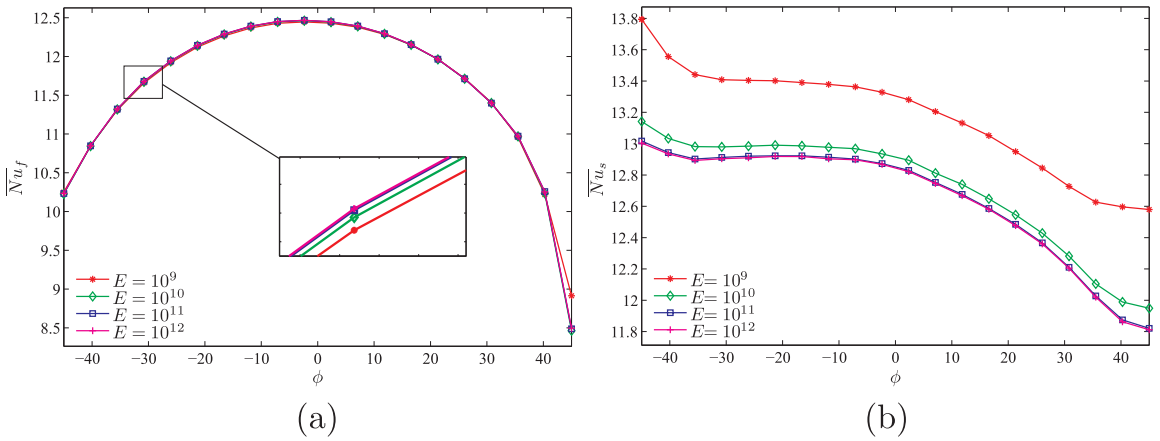

Fig. 21. Variation of the average Nusselt number on (a) the inclined left wall and (b) the solid fin with ϕ for different E at $K_r = 10$, $A = 0.1$ and $H = 0.5$.

reduction occurs for positive values of the inclination angle. It should be noted that the value $\phi = 45$ characterizes a more complicated time dependence for $\overline{Nu}_f$ and $\overline{Nu}_s$.

Fig. 21 demonstrates the effects of ϕ and E on the average Nusselt numbers. As it has been mentioned above, a growth of the dimensionless Young's modulus leads to a rise of $\overline{Nu}_f$, while $\overline{Nu}_s$ decreases. As for the sloping walls inclination angle, a growth of this angle from −45 to 45 results in a reduction of the average Nusselt number at the fin surface, while $\overline{Nu}_f$ increases for $-45 < \phi < 0$ and it decreases for $0 < \phi < 45$.

The effects of the oscillations amplitude and the sloping walls inclination angle on the considered average Nusselt numbers are shown in Fig. 22. A growth of the oscillations amplitude leads to a rise of the average Nusselt number at the left wall heater surface, while $\overline{Nu}_s$ changes non-monotonically.

Fig. 23 shows the effects of the left wall heater length and the sloping walls inclination angle on the average Nusselt numbers. A growth of the left wall heater length leads to a heat transfer enhancement for the left wall heater and fin. It should be noted that a more essential impact of H on $\overline{Nu}_f$ occurs for $0.6 < H < 0.9$.

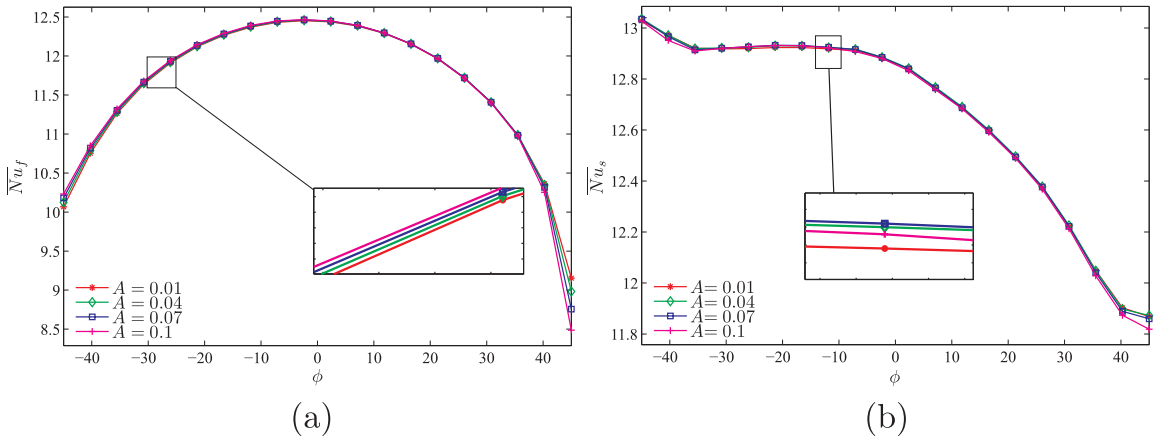

Fig. 22. Variation of the average Nusselt number on (a) the inclined left wall and (b) the solid fin with ϕ for different A at $K_r = 10$, $E = 10^{11}$ and $H = 0.5$.

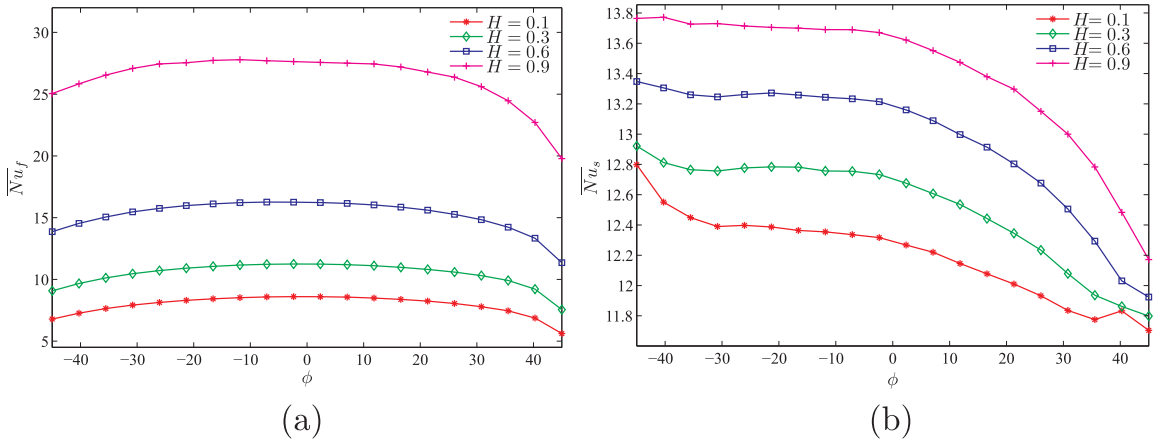

Fig. 23. Variation of the average Nusselt number on (a) the inclined left wall and (b) the solid fin with ϕ for different H at $K_r = 10$, $E = 10^{11}$ and $A = 0.1$.

5. Conclusions

In the present study, the Galerkin finite element method combined with the Arbitrary Lagrangian-Eulerian procedure is used to study the unsteady laminar natural convection in a differentially-heated oblique cavity with a flexible oscillating heat-conducting fin. The governing equations in dimensionless form have been formulated using the Arbitrary Lagrangian-Eulerian procedure. The detailed results for the streamlines, isotherms, fluid flow rate, and the average Nusselt numbers are shown graphically for wide ranges of the dimensionless time, thermal conductivity ratio, non-dimensional Young's modulus, oscillating amplitude, left wall heater length, and the inclination angle of sloping walls. The important conclusions for this investigation are as follows:

1. A growth of the thermal conductivity ratio leads to a rise of the average Nusselt number at the fin surface. At the same time, for the left wall heater $\overline{Nu}_f$ does not depend on K_r for $t < 10^{-3}$, while for $t > 10^{-3}$ a growth of the thermal conductivity ratio leads to a diminution of the average Nusselt number at the left wall heater element.
2. An increase in the dimensionless Young's modulus results in the convective flow intensification for $10^9 \leqslant E \leq 10^{10}$, while for $10^{10} \leqslant E \leq 10^{12}$ one can find a weak attenuation of the convective flow. A rise of E leads to an increase in $\overline{Nu}_f$. At the same time, $\overline{Nu}_s$ decreases with the dimensionless Youngs modulus.
3. A rise of the oscillation amplitude for the free end of the elastic fin leads to a growth of the amplitude for the fluid flow rate and the heat transfer rates, while the time averaging of the fluid flow rate and the average Nusselt number at the fin surface leads to a reduction of these values with A. At the same time, the time averaging of the average Nusselt number at the heater surface increases with the oscillation amplitude.
4. A growth of the absolute value of the sloping walls inclination angle leads to the reduction of $\overline{Nu}_f$. A more essential diminution of $\overline{Nu}_f$ with $|\phi|$ occurs for $10^{-8} \leqslant t < 10^{-4}$, while for $t > 10^{-4}$ this reduction is not so significant. In the case of $\overline{Nu}_s$, the influence of ϕ is visible for $10^{-6} \leqslant t < 10^{-4}$. An increase in the inclination angle from −45 to 45 characterizes a diminution of the average Nusselt number at the fin surface. Moreover, a more essential reduction occurs for positive values of the inclination angle.

Acknowledgments

The work was supported by the grant GSP/1/2015/SG04/UKM/01/1. Also, M.A. Sheremet acknowledges the financial support from the Ministry of Education and Science of the Russian Federation (Project Number 13.6542.2017/6.7). We thank the respected reviewers for their constructive comments which clearly enhanced the quality of the manuscript.

References

[1] S. Ostrach, Natural convection in enclosures, J. Heat Transfer 110 (4-B) (1988) 1175–1190.
[2] H.J. Bungartz, M. Schäfer, Fluid-structure interaction: modelling, simulation, optimisation; vol. 53. Springer Science & Business Media; 2006.
[3] J.F. Sigrist, Fluid-Structure Interaction: An Introduction to Finite Element Coupling, John Wiley & Sons, 2015.

[4] Franci A. Unified Lagrangian formulation for fluid and solid mechanics, fluid-structure interaction and coupled thermal problems using the PFEM. Springer; 2016.
[5] Basting S, Birken P, Canic S, Colciago C, Deparis S, Forti D, et al. Fluid-structure interaction: modeling, adaptive discretisations and solvers; vol. 20. Walter de Gruyter GmbH & Co KG; 2017.
[6] Richter T. Fluid-structure Interactions: Models, Analysis and Finite Elements; vol. 118. Springer; 2017.
[7] H.F. Öztop, I. Dagtekin, Mixed convection in two-sided lid-driven differentially heated square cavity, Int. J. Heat Mass Transfer 47 (8-9) (2004) 1761–1769.
[8] F. Talebi, A.H. Mahmoudi, M. Shahi, Numerical study of mixed convection flows in a square lid-driven cavity utilizing nanofluid, Int. Commun. Heat Mass Transfer 37 (1) (2010) 79–90.
[9] E. Abu-Nada, A.J. Chamkha, Mixed convection flow in a lid-driven inclined square enclosure filled with a nanofluid, Eur. J. Mech-B/Fluids 29 (6) (2010) 472–482.
[10] A. Rashad, S. Abbasbandy, A.J. Chamkha, Mixed convection flow of a micropolar fluid over a continuously moving vertical surface immersed in a thermally and solutally stratified medium with chemical reaction, J. Taiwan Inst. Chem. Eng. 45 (5) (2014) 2163–2169.
[11] G. Ramesh, A. Chamkha, B. Gireesha, Boundary layer flow past an inclined stationary/moving flat plate with convective boundary condition, Afrika Matematika 27 (1-2) (2016) 87–95.
[12] M. Raju, A. Chamkha, J. Philip, S. Varma, Soret effect due to mixed convection on unsteady magnetohydrodynamic flow past a semi infinite vertical permeable moving plate in presence of thermal radiation, heat absorption and homogenous chemical reaction, Int. J. Appl. Computat. Math. 3 (2) (2017) 947–961.
[13] A.J. Chamkha, A.M. Rashad, M.A. Mansour, T. Armaghani, M. Ghalambaz, Effects of heat sink and source and entropy generation on MHD mixed convection of a Cu-water nanofluid in a lid-driven square porous enclosure with partial slip, Phys. Fluids 29 (5) (2017) 052001.
[14] A.I. Alsabery, M.A. Ismael, A.J. Chamkha, I. Hashim, Mixed convection of Al_2O_3-water nanofluid in a double lid-driven square cavity with a solid inner insert using buongiornos two-phase model, Int. J. Heat Mass. Transf. 119 (2018) 939–961.
[15] A.K. Kareem, S. Gao, Computational study of unsteady mixed convection heat transfer of nanofluids in a 3D closed lid-driven cavity, Int. Commun. Heat Mass Transfer 82 (2017) 125–138.
[16] X. Shi, J. Khodadadi, Fluid flow and heat transfer in a lid-driven cavity due to an oscillating thin fin: transient behavior, Trans. ASME-C-J. Heat Transfer 126 (6) (2004) 924–930.
[17] X. Shi, J. Khodadadi, Periodic state of fluid flow and heat transfer in a lid-driven cavity due to an oscillating thin fin, Int. J. Heat Mass Transf. 48 (25) (2005) 5323–5337.
[18] C.H. Ku, Flexible heat transfer assembly, 2015. US Patent App. 14/084284.
[19] A.K. Soti, R. Bhardwaj, J. Sheridan, Flow-induced deformation of a flexible thin structure as manifestation of heat transfer enhancement, Int. J. Heat Mass Transf. 84 (2015) 1070–1081.
[20] F. Selimefendigil, H.F. Öztop, Analysis of MHD mixed convection in a flexible walled and nanofluids filled lid-driven cavity with volumetric heat generation, Int. J. Mech. Sci. 118 (2016) 113–124.
[21] F. Selimefendigil, H.F. Öztop, A.J. Chamkha, Fluid-structure-magnetic field interaction in a nanofluid filled lid-driven cavity with flexible side wall, Eur J Mech-B/Fluids 61 (2017) 77–85.
[22] M. Ghalambaz, E. Jamesahar, M.A. Ismael, A.J. Chamkha, Fluid-structure interaction study of natural convection heat transfer over a flexible oscillating fin in a square cavity, Int. J. Therm. Sci. 111 (2017) 256–273.
[23] F. Selimefendigil, H.F. Öztop, Laminar convective nanofluid flow over a backward-facing step with an elastic bottom wall, J. Therm. Sci. Eng. Appl. 10 (4) (2018) 041003.
[24] F. Selimefendigil, H.F. Öztop, A.J. Chamkha, Analysis of mixed convection and entropy generation of nanofluid filled triangular enclosure with a flexible sidewall under the influence of a rotating cylinder, J. Therm. Anal. Calorim. https (2018) //doi–018-7317-5.
[25] A. Raisi, I. Arvin, A numerical study of the effect of fluid-structure interaction on transient natural convection in an air-filled square cavity, Int. J. Therm. Sci. 128 (2018) 1–14.
[26] F. Selimefendigil, H.F. Oztop, A.J. Chamkha, MHD mixed convection in a nanofluid filled vertical lid-driven cavity having a flexible fin attached to its upper wall, J. Therm. Anal. Calorimetry 2018; https://doi.org/10.1007/s10973-018-7036-y.
[27] M.A. Ismael, H.F. Jasim, Role of the fluid-structure interaction in mixed convection in a vented cavity, Int. J. Mech. Sci. 135 (2018) 190–202.
[28] A.I. Alsabery, A.J. Chamkha, H. Saleh, I. Hashim, Transient natural convective heat transfer in a trapezoidal cavity filled with non-Newtonian nanofluid with sinusoidal boundary conditions on both sidewalls, Powder Technol. 308 (2017) 214–234.
[29] A. Baïri, E. Zarco-Pernia, J.M.G. De María, A review on natural convection in enclosures for engineering applications. the particular case of the parallelogrammic diode cavity, Appl. Therm. Eng. 63 (1) (2014) 304–322.
[30] J.M. Hyun, B.S. Choi, Transient natural convection in a parallelogram-shaped enclosure, Int. J. Heat Fluid Flow 11 (2) (1990) 129–134.
[31] H.S. Han, J.M. Hyun, Buoyant convection in a parallelogrammic enclosure filled with a porous medium-general analysis and numerical simulations, Int. J. Heat Mass Transf. 51 (11) (2008) 2980–2989.
[32] A. Baïri, J.G. de María, N. Laraqi, Transient natural convection in parallelogrammic enclosures with isothermal hot wall. Experimental and numerical study applied to on-board electronics, Appl. Therm. Eng. 30 (10) (2010) 1115–1125.
[33] M. Ghalambaz, M.A. Sheremet, I. Pop, Free convection in a parallelogrammic porous cavity filled with a nanofluid using Tiwari and Das' nanofluid model, PloS one 10 (5) (2015) e0126486.
[34] R. Nayak, S. Bhattacharyya, I. Pop, Numerical study on mixed convection and entropy generation of Cu-water nanofluid in a differentially heated skewed enclosure, Int. J. Heat Mass Transf. 85 (2015) 620–634.
[35] A.I. Alsabery, H. Saleh, I. Hashim, P.G. Siddheshwar, Transient natural convection heat transfer in nanoliquid-saturated porous oblique cavity using thermal non-equilibrium model, Int. J. Mech. Sci. 114 (2016) 233–245.
[36] A.I. Alsabery, H. Saleh, I Hashim, Effects of viscous dissipation and radiation on MHD natural convection in oblique porous cavity with constant heat flux. Adv. Appl. Math. Mech. 2017b;9(2):463–484.
[37] D. Das, M. Roy, T. Basak, Studies on natural convection within enclosures of various (non-square) shapes – a review, Int. J. Heat Mass Transf. 106 (2017) 356–406.
[38] Sun F. Investigations of smoothed particle hydrodynamics method for fluid-rigid body interactions. Ph.D. thesis. University of Southampton; 2013.
[39] A.C. Hindmarsh, P.N. Brown, K.E. Grant, S.L. Lee, R. Serban, D.E. Shumaker, et al., SUNDIALS: Suite of nonlinear and differential/algebraic equation solvers, ACM Transactions on Mathematical Software (TOMS) 31 (3) (2005) 363–396.
[40] T. Nishimura, M. Shiraishi, F. Nagasawa, Y. Kawamura, Natural convection heat transfer in enclosures with multiple vertical partitions, Int. J. Heat Mass Transf. 31 (8) (1988) 1679–1686.
[41] S.W. Churchill, Free convection in layers and enclosures, in: G.f. hewitt, exec. ed,. Heat exchanger design handbook, Section 258, Begell House, New York, 2002.